The Murchison Greenstone Belt, South Africa: Accreted slivers with contrasting metamorphic conditions

Sylvain Block, Jean-François Moyen, Armin Zeh, Marc Poujol, Justine Jaguin, Jean-Louis Paquette

THE MURCHISON GREENSTONE BELT, SOUTH AFRICA: ACCRETED SLIVERS WITH CONTRASTING METAMORPHIC CONDITIONS

Sylvain Block[a,b]
Jean-François Moyen[a,b]
Armin Zeh[c]
Marc Poujol[d]
Justine Jaguin[d]
Jean-Louis Paquette[a]

a *Laboratoire Magmas et Volcans, UMR 6524 CNRS. Université Blaise Pascal, Rue Kessler, 63038 Clermont-Ferrand, France.*
b *Université Jean Monnet, 23 rue du Dr Paul Michelon, 42023 Saint-Étienne. France.*
c *Institut für Geowissenschaften, Altenhöfer Allee 1, D-60438 Frankfurt am Main, Germany.*
d *Géosciences Rennes, UMR CNRS 6118, Université de Rennes 1, Campus de Beaulieu, 35042 Rennes CEDEX, France.*

Corresponding author :
Sylvain Block
Université Jean Monnet, 23 rue du Dr Paul Michelon, 42023 Saint-Étienne. France.
Tel : +33(0)621333525
sylvain.block@gmail.com

Abstract

This paper presents new petrological and geochronological data for the ~3.09-2.92 Ga Murchison Greenstone Belt (MGB), located in South Africa's Kaapvaal Craton, and discusses their geotectonic implications. The MGB is made of three tectono-metamorphic units: the Silwana Amphibolites, the Murchison Unit and the La France Formation. They underwent contrasting clockwise pressure-temperature-deformation (P-T-D) histories, and are separated from each other by relatively narrow, high-strain shear zones, with a sinistral, transpressive top-to-the-south movement, consistent with the deformation patterns observed throughout the belt. These patterns are explained by a N-S compressional stress field, affecting the Murchison Belt between 2.97 and 2.92 Ga. Results of new petrological investigations indicate that ultramafic to felsic volcano-sedimentary rocks of the Murchison Unit underwent a greenschist- to lower-amphibolite-facies metamorphism at maximum P—T conditions of 5.6

± 0.6 kbar at 570°C, along a relatively hot, minimum apparent geotherm of ~30°C/km. In contrast, the Silwana Amphibolites and the La France Formation were metamorphosed at much higher peak metamorphic conditions of 8.7-10 kbar, 630-670°C, and 8-9 kbar, 600-650 °C respectively, and require a colder apparent geotherm of ~20°C/km. A retrograde, nearly isothermal-decompression P—T path followed by isobaric cooling is also inferred for the La France Formation. The timing of the structural-metamorphic overprint is bracketed between 2.97 and 2.90 Ga, which is constrained by U-Pb zircon ages of a syn-deformation granite within the Murchison Unit and the post-deformation Maranda granite, respectively. Monazite and xenotime from La France metapelites yield much younger ages of ca. 2.75 Ga, with few inherited components at 2.92 Ga. They point to a later activation of the MGB, perhaps related with tectono-thermal events in the Rooiwater Complex and the Pietersburg Greenstone Belt. The relatively cold apparent geotherms recorded in the Silwana and La France rocks, the contrasted peak P—T conditions between the different units, and the near isothermal decompression of the La France Formation indicate that the Kaapvaal craton crust must have been cold enough to enable significant crustal thickening and strain localisation along narrow shear zones and, as a consequence, fast tectonic juxtaposition of rocks metamorphosed at different crustal depths. These features are similar to those observed along Palaeozoic or modern day, oblique subduction-collision zones, but different to those of hot Archaean provinces. We therefore interpret the MGB as representing part of an oblique collision-zone between two terrains of the Kaapvaal craton: the Witwatersrand and Pietersburg terrains.

Keywords : Metamorphism, Archaean tectonics, Murchison Greenstone Belt, Kaapvaal craton.

1. Introduction

Many tectonic studies on various Archaean cratons have reported structural features in volcano-sedimentary belts that differ from younger Proterozoic and Phanerozoic orogenic belts (e.g. Bouhallier et

al., 1993, 1995; Choukroune et al., 1995, 1997; Chardon et al., 1996, 1998, 1999). Linear fold and thrust belts, strain localisation along crustal scale faults, juxtaposition of contrasted metamorphic domains forming "paired metamorphic belts" (e.g., the Mesozoic Ryoke-Sanbagawa belts in Japan, Miyashiro, 1961; Brown, 2010 and references therein), tectonically driven exhumation processes, as well as features that are typical of subduction, such as ophiolites, accretionary prisms and blueschist-facies to Ultra-High-Pressure-facies metamorphism, are widely recognised in modern orogens. On the other hand, ubiquitous craton scale shear zones, dome and basin strain patterns, deformation distribution on a regional scale, and the relative homogeneity of erosion levels and metamorphic gradients are characteristic of many Archaean granite-greenstone provinces (Binns et al., 1976; Park, 1992; Chardon et al., 2008, 2009). The description of features in Archaean provinces interpreted to be related to subduction and modern-style accretion tectonics has fed the debate on the onset of plate tectonics and on the evolution of tectonic regimes through time (e.g. Komiya et al., 1999; Kusky et al., 2001; de Wit, 2004; Condie and Kröner, 2008; Cawood et al., 2009); and the recognition of contrasted tectono-metamorphic signatures between modern and Archaean orogens led authors to invoke secular changes in the thermal regime of the Earth as the factor driving the shift from one tectonic style to another (e.g. Komiya et al., 2002; Brown, 2007; Gapais et al, 2009; Sizova et al., 2010). A wide range of models were proposed to account for the features observed in Archaean provinces. An intellectual framework defined by two "end-member" models, with a hot and weak lithosphere in the Archaean as opposed to a cold and strong lithosphere in the Proterozoic and Phanerozoic eras has been widely adopted. However, given the wide variation in the rheological properties of Phanerozoic lithospheres (Watts and Burov, 2003 and refs. therein), one can expect to be confronted to such geographical disparities in Archaean cratons.

The heat budget of the lithosphere is a major control of its rheological properties, and as a consequence, of the dominant tectonic regime in the crust. Metamorphic rocks record evidence of the pressure and temperature evolution with time, which reflects the thermal environment under which the constituent mineral assemblages equilibrated. Spatial distribution of peak P—T conditions provide information on the spatial variation in thermal regimes; hence metamorphic studies are an important tool to investigate the

tectonic style of Archaean provinces. Although metamorphic studies, coupled with structural and geochronological constraints, have contributed greatly to our understanding of modern orogenic processes (e.g. Miyashiro, 1961; Ernst, 1973, 1975, 1988; Chopin, 1984; Smith, 1984; Brown, 2009), metamorphism across Archaean granite–greenstone terrains has been comparatively under-studied. Consequently, the lack of well-constrained metamorphic studies has hampered the development of a geodynamic framework for the formation of granite–greenstone terrains. It has also led to the generalisation in the literature of implicit assumptions on Archaean metamorphism, as some observations relevant to specific Archaean provinces are taken to be a general rule.

Most granite–greenstone terrains are reported to have undergone metamorphism along high-Temperature, low-Pressure apparent geothermal gradients. Metamorphic conditions are generally described as isobaric across hundreds of kilometres, with isotherms parallel to the surface, or as grading progressively from low-grade greenschist-facies to granulite-facies across kilometres-large and hundreds of kilometres-long shear zones, where strain is distributed rather than localised (Grambling, 1986; Collins and Vernon, 1991; Percival et al.,1992; Percival et al., 1994; Caby et al., 2000). Variations in metamorphic grade in Archaean granite–greenstone terrains are frequently attributed to contact metamorphism linked to the emplacement of granitoid bodies, or as the result of a "crustal overturn" (Van Kranendonk, 2002). However, an increasing number of studies provide evidence for disparities in metamorphic patterns between Archaean terrains. High P-low T metamorphism (18-20 kbar, 630°C) is reported from the Indian Bundelkhand Craton at ca. 2.78 Ga (Saha et al., 2011); ca. 2.72 Ga eclogite-facies metamorphism is recorded in the Belomorian belt of Russia (Volodichev, 2004; Brown, 2009; Mints et al., 2010). High metamorphic gradients between terrains metamorphosed at different depths, and juxtaposed along planar tectonic structures that localised deformation, are described in the Palaeoarchaean Barberton Greenstone Belt (BGB), in the east of the Kaapvaal craton, South Africa (Kisters et al., 2003; Diener et al., 2005; Moyen, 2006) and in the Mesoarchaean Point Lake orogen of the Slave Province, Canada (Kusky et al. 1991).

This study aims to unravel the tectono-thermal history of the northwestern part of the Archaean Kaapvaal Craton in South Africa. In order to do so, the metamorphic conditions across the Murchison

Greenstone Belt, the nature of the contacts between the distinct tectono-metamorphic units, and the timing of the structural-metamorphic and magmatic processes were investigated. By coupling the different information, we intend to bring new insights into the geodynamic evolution that led to the formation of the MGB and to contribute to a broader understanding of Archaean tectonics.

2. Geological setting of the MGB

2.1. Regional context and geochronological constraints

The ENE-WSW trending Murchison Greenstone Belt is one of the volcano-sedimentary belts of the Archaean Kaapvaal craton of South Africa (Brandl et al., 2006; Robb et al., 2006) (Fig. 1). It is situated about 200 km north of the ca. 3.5-3.2 Ga Barberton Greenstone Belt (e.g. Kröner et al., 1991, 1992, 1996; Kamo and Davis, 1994; Dziggel et al., 2002), and about 80 km south of the 3.2-2.8 Ga Giyani Greenstone Belt (Kröner et al, 2000). It extents for ~140 km ENE-WSW, 15 – 20 km N-S, and is unconformably overlain by the Neoarchaean to Palaeoproterozoic sediments of the Transvaal Supergroup (Burger and Coertze, 1973; Altermann and Nelson, 1998) at its western extremity. Furthermore, it is located along the "Murchison-Thabazimbi Lineament" (Du Plessis, 1990), which is defined on the basis of geophysical data and interpreted to form an important terrain boundary in the northern Kaapvaal craton, separating the Witwatersrand terrain to the south from the Pietersburg terrain to the north (Good and de Wit, 1997; Anhaeusser, 2006, Zeh et al., 2009).

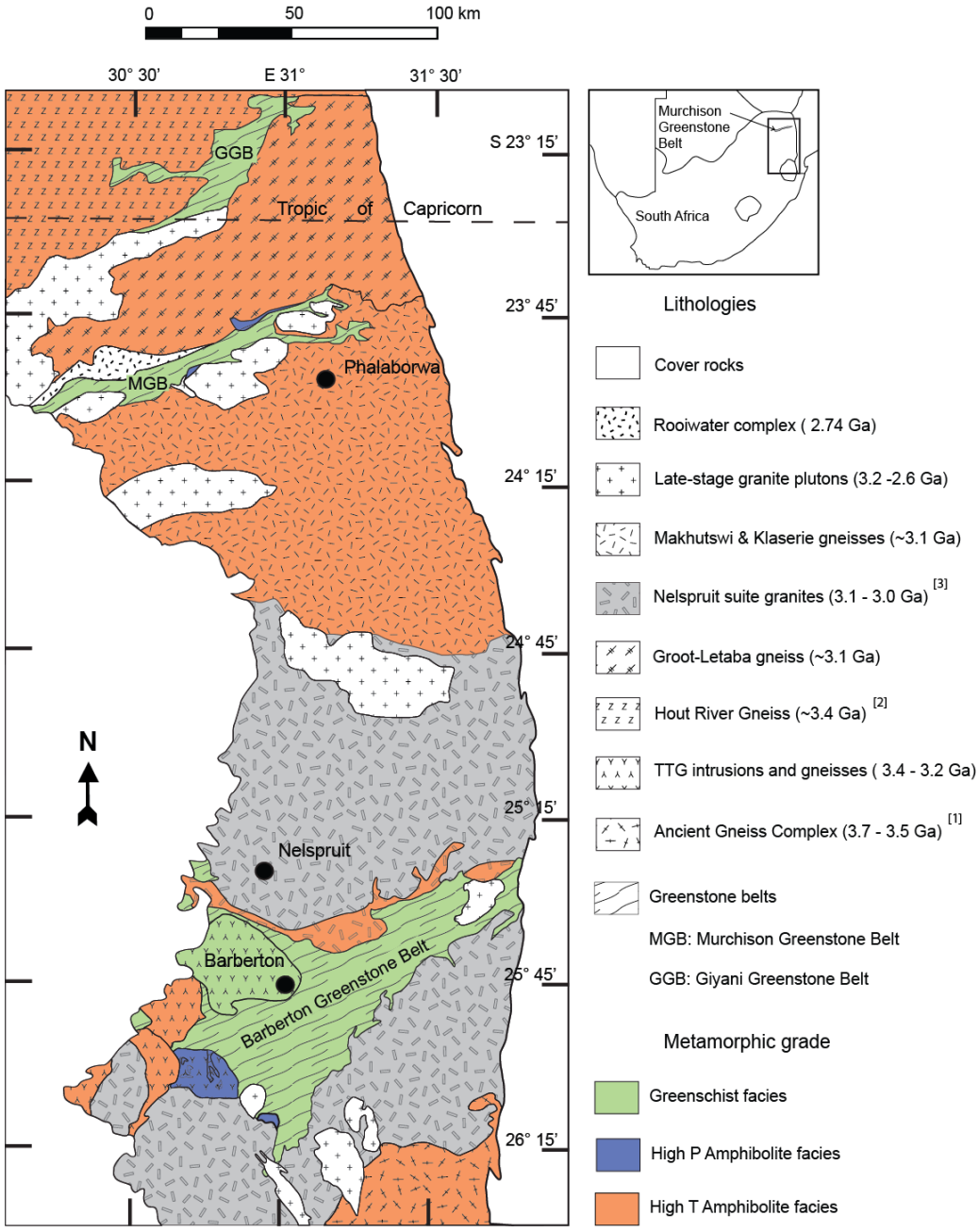

Figure 1:

Simplified geologic map of the north-eastern part of the Kaapvaal craton. Different colours represent domains with different metamorphic grades, inferred from sparse field observations and data from the literature. [1]: Kröner and Tegtmeyer (1994); Compston and Kröner (1988), [2]: Kamo and Davis (1994), [3]: Brandl and Kröner (1993); Kröner et al. (2000). See text for other references.

At its northern margin, the supracrustal rocks of the MGB are bounded by the Rooiwater Complex and the Groot Letaba Gneisses. The Rooiwater Complex (Vearncombe et al., 1997) represents a mostly undeformed layered mafic intrusion emplaced at a minimum age of 2.74 Ga (Poujol et al. 1996) and

subsequently intruded by mafic dykes at 2.61 Ga (Zeh et al., 2009). Field evidence however suggest that this age may correspond to a late resetting of geochronometers, and the emplacement age of the Rooiwater complex is likely to be significantly older (Vearncombe, 1992). The contact between the Rooiwater Complex and the MGB is tectonically reworked (Vearncombe, 1992). The Groot Letaba Gneisses (Brandl and Kröner, 1993) comprise a series of locally migmatised dark-grey gneisses, tonalites and trondjhemites. They were mostly emplaced at ca. 3180 – 3000 Ma, with the exception of some ca. 2885 ± 4 Ma discordant leucogneisses (Brandl and Kröner, 1993). The basement directly to the south of the MGB is made of granitoids (TTGs) of the French Bob's Mine, emplaced 3228 ± 12 Ma ago (Poujol et al. 1996); and by younger intrusive granitoids of ca. 3110 – 3060 Ma (Brandl and Kröner, 1993 ; Poujol and Robb, 1999). The southern margin of the MGB was affected by the episodic intrusion of granite plutons and pegmatites of the Voster Suite, at ca. 3020, 2970, 2900, 2820 and 2680 Ma, respectively for the Baderoukwe, Discovery, Maranda, Willie, Mashishimale plutons, and associated intrusions (Fig. 2) (Poujol et al 1996; Poujol and Robb, 1999; Poujol, 2001; Zeh et al., 2009). Published geochronological data indicate that the supracrustal sequence of the MGB formed over a period of more than 100 Ma, between ca. 3090 and 2970 Ma (Poujol et al., 1996, Poujol et al., 2001).

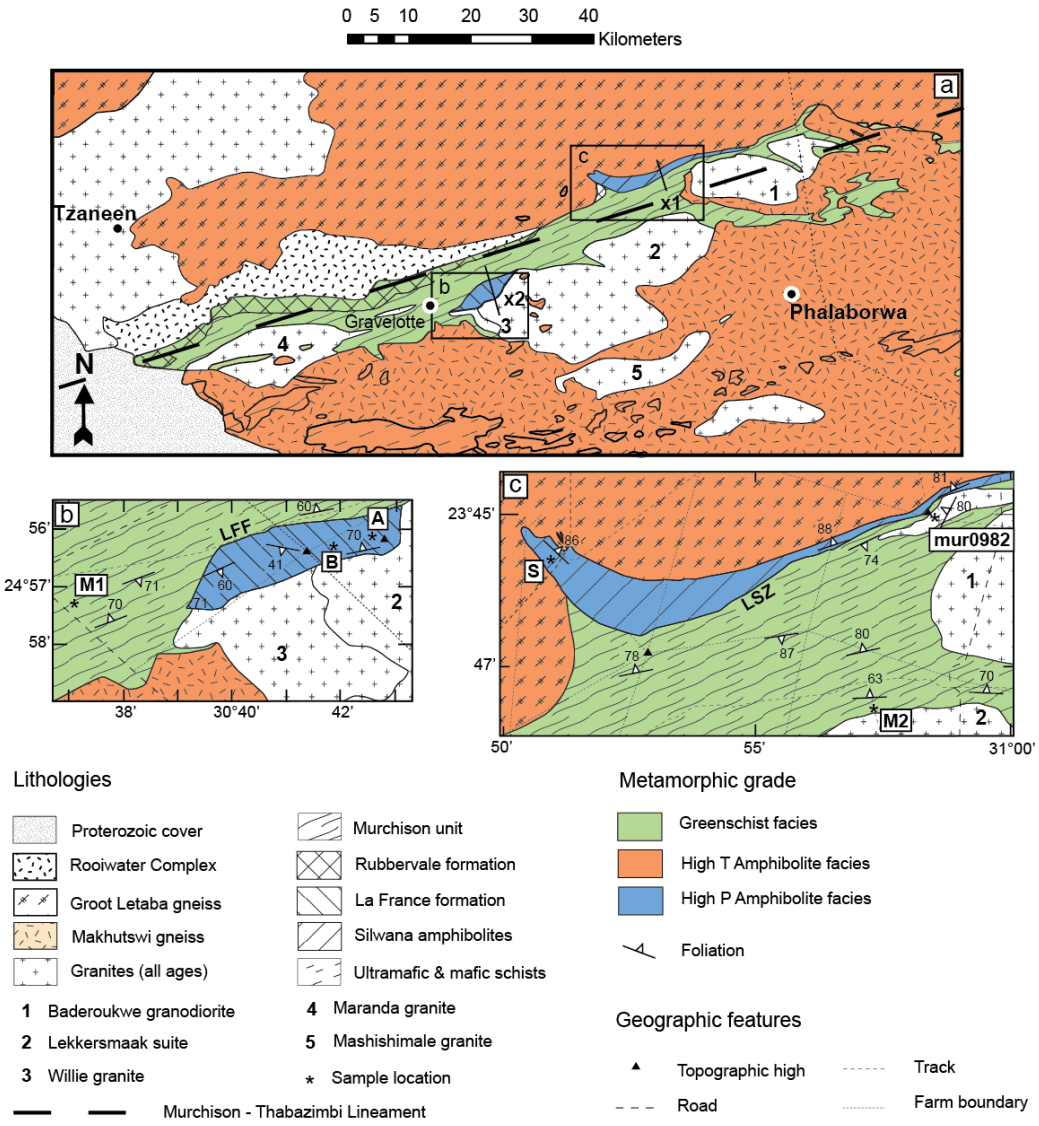

Figure 2:

(a) Simplified geologic and metamorphic map of the Murchison Greenstone Belt and its surroundings. (b, c) Detailed maps with the location of samples (A, B, S, M1, M2 and mur0982) discussed in the text, modified from Vearncombe et al. (1992). The lines marked with x_1 and x_2 correspond to the cross section shown in Fig. 9. LFF = La France Fault, LSZ = Letaba Shear Zone.

2.2. Structural-Metamorphic Units of the MGB

Based on structural and lithological criteria, Vearncombe et al. (1992) subdivided the MGB into four major, ENE-WSW-striking lithostratigraphic domains (Fig. 2):

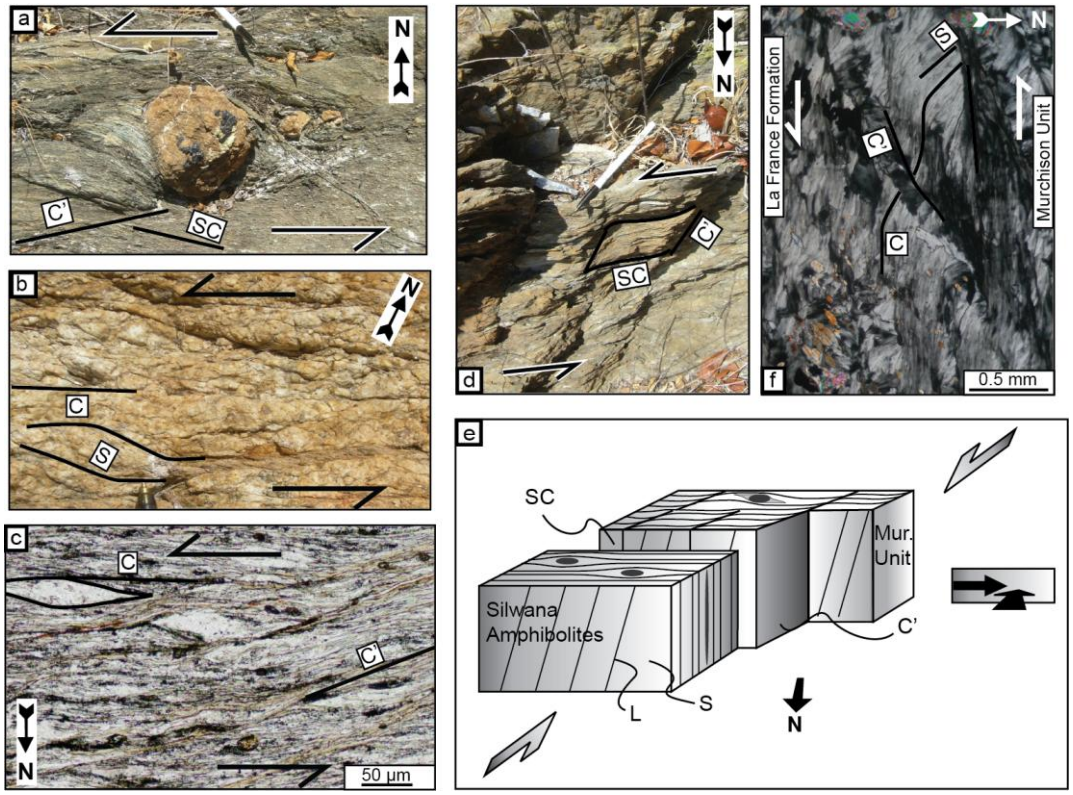

Figure 3:

Fabrics at or near to the sheared contacts between the different terrains of the MGB. (a). Asymmetric pressure shadow zones around a carbonate nodule in a mylonitic carbonate schists of the Murchison Unit, in the Letaba Shear Zone. (b) S – C fabrics in a deformed granite within the Letaba Shear Zone. (c) Microstructures observed in the quartz-chlorite schists of the Letaba Shear Zone include C' shear bands and mineral fish. (d) S-C - C' planes in quartz-chlorite schists of the Murchison Unit, in the Letaba Shear Zone. The kinematic indicators in (a), (b), (c) and (d) provide evidence for sinistral motion along the shear zone. (e) Synopsis of the structures observed along the Letaba shear zone. The flattening fabric in the Silwana amphibolites, that formed under upper- amphibolite facies conditions, occurs in close contact with mylonitised schists of the Murchison Unit, which provide evidence for a sinistral strike-slip under greenschist facies conditions. The latter is interpreted to have occurred in a transpressive setting and was accompanied by a top-to-the-south motion. (f) S – C – C' fabrics in a chlorite schists of the Murchison Unit, near the contact with the La France Formation, provide evidence for top-to-the-south motion. The C planes are subvertical.

The largest lithological domain of the MGB, hereafter referred to as the **"Murchison Unit"**, includes the MacKop, Weigel, Leydsdorp and Mulati formations of the South African Committee for Stratigraphy (SACS) (1980) nomenclature. It consists of mafic and ultramafic volcanic rocks along with volcano-

sedimentary and sedimentary rocks. The most representative lithologies of the domain are mafic quartz-chlorite and albite-chlorite-actinolite schists, locally pillowed. The volcano-sedimentary rocks are locally interbedded with BIFs and with aluminous quartzites and conglomerates. The clastic sediments form prominent ridges, often corresponding to synform limbs in the central part of the MGB. Massive carbonates and carbonate schists crop out mostly along a high-strain shear zone in the centre of the belt, flanked by quartzite ridges to the north: the Antimony Line (Viljoen et al., 1978; Vearncombe, 1988a, 1992), which hosts Sb (± Au) mineralisation. Serpentinite lenses occur in the southern part of the belt. Stratigraphic relationships within this unit remain unclear, as contacts between formations are tectonic in nature (Vearncombe, 1992). U-Pb zircon ages provide evidence that the Weigel Formation volcanics were emplaced at ca. 3.09 Ga, while a maximum age of deposition for the MacKop conglomerate was found to be ca. 3.08 Ga old (Poujol et al., 1996).

The **Rubbervale Formation** is exposed along the northwestern flank of the MGB. It comprises quartz-porphyroclastic schists, along with felsic lavas, tuffs and breccias. This formation also hosts the major VMS-type deposit of the so-called ‘Cu-Zn” line (Schwarz-Schampera et al., 2010). Emplacement of the Rubbervale formation was dated at ca. 2.97 Ga (Brandl et al. 1996 ; Poujol et al. 1996 ; Poujol 2001).

The third unit, the **Silwana Amphibolites** (Vearncombe et al., 1992; part of the Rubbervale formation in the SACS terminology), is exposed in the north-eastern part of the MGB, and represent a 0.1-1.5 km wide sliver of amphibolites, rarely garnet-bearing, displaying a centimetric layering.

La France Formation (Vearncombe et al., 1992, SACS terminology) mostly consists of quartzite and kyanite- staurolite- garnet-bearing biotite micaschists.

Vearncombe et al. (1988b) and Vearncombe (1992) stated that the Silwana Amphibolites and the rocks of the La France Formations experienced a higher degree of metamorphism than the rocks of the Murchison Unit and Rubbervale Formation, which together form the core of the MGB (Fig. 2). Metamorphic P—T conditions were estimated to be > 5kbar, 550-650°C for the La France Formation, while field

observations qualitatively suggested a higher grade metamorphic conditions in the Silwana Amphibolites compared to the Murchison Unit.

Table 1:

Summary of the mineral assemblages and textures developed in the different formations of the MGB.

Terrain	Rock type	Outcrop occurrence	Mineral assemblages	Texture	Sample
La France Formation	Gt- St-bearing micaschist	Bt-schist with thin metamorphic banding, crenulated. Protruding elongated Gt and St	Peak (syn-D_2): Gt + St + Bt + Ms + Q Post-peak: Bt, Hem	Large Gt and St porphyroblasts, thin Bt beds, crenulated.	A
La France Formation	Ky (± St)-bearing micaschist	Bt-schist with thin metamorphic banding. Protruding elongated Ky.	Peak (syn-D_2): Ky + Bt + Ms + Pl ± St ± Ilm ± Ru + Q Retrograde: Bt + Sill + Pl + Crd / Bt + Chl + Ms + St ± Ky Accessory : Mnz, Xno	Large Ky porphyroblasts, elongated parallel to Bt beds. Retrograde Crd, Bt - Chl - Ms simplectite, St	B
Murchison Unit	Act-bearing metabasite	Green metabasite, no pervasive tectonic fabric	Peak : Act + Ab + Chl + Ep + Sph	Garbenscheifer texture : needle-shaped Act, Chl in late shear bands	M1
Murchison Unit	Aluminous quartzite	Fine grained quartzite with well developped metamorphic cleavage, parallel to micaceous bedding	Peak : Gt + Bt + Ms + Q Retrograde: Chl	Thin aligned Ms and Bt beds with small Gt, intercalated with protogranular quartz beds	M2
Silwana Amphibolites	Gt- Hbl-bearing amphibolite	Dark, fine grained, massive « amphibolitic gneiss » with occasional garnet-bearing layers.	Peak: Hbl + Pl + Gt + Bt + Ilm + Q Retrograde: Chl, Ep Accessory: Ap, Calc	Equigranular texture with aligned Hbl. Intercalation of Hbl and recristallised Pl and quartz beds. Gt porphyroblasts with Ilm and Hbl inclusions	S

2.3. Contact zones between the units of the MGB

The different units of the MGB are separated from each other by large-scale ductile shear zones. A detailed structural study of the MGB is beyond the scope of this paper and only a brief review of the nature of the contacts is presented here. A description of the regional strain field and the tectonics of the MGB are given in Vearncombe (1988b); Kusky and Vearncombe (1997) and Jaguin et al. (2012).

2.3.1. The Letaba Shear Zone

To the north-east of the MGB, the Letaba Shear Zone (LSZ) separates the Silwana Amphibolites from low-grade, quartz-chlorite and carbonate schists of the Murchison Unit. The contact is very sharp and shows signs of a tectonic melange. The Silwana Amphibolites display a penetrative flattening fabric formed under amphibolite-facies conditions. The cleavage is subvertical and bears a steep (pitch >75°) easterly plunging mineral elongation lineation. Asymmetric shear sense indicators are rare within this formation: pressure shadow zones around garnet porphyroblasts are symmetrical, and no shear bands were observed in thin sections. Towards the contact with the Silwana Amphibolites, the Murchison Unit schists display a mylonitic microstructure and a significant grain size reduction. The mylonites exhibit an NE-SW cleavage, parallel to the contact between the two formations. The cleavage has a moderate to sub-vertical dip to the south and carries a mineral elongation lineation dipping moderately (pitch > 40°) to the east. Asymmetric shear sense indicators, such as pressure shadow zones around primary carbonate nodules consistently point to a sinistral shear (Fig. 3a). The same shear direction is also reflected by SC-C'-fabrics and extensional crenulation cleavages (Berthé at al., 1979; Platt and Vissers, 1980), indicative of stretching parallel to the foliation, which are well developed within the mylonitised quartz-chlorite-schists (Fig. 3c, d). At the "Witkop" locality (near sample mur0982 in Fig. 2), where the relationships between the different units are clearly exposed, a deformed granite intrudes the greenschist-facies mylonites of the Murchison Unit. No contact metamorphism was observed in the quartz-chlorite schists around the granite body. The granite displays well-expressed C-S structures (Fig. 3b). S and C surfaces have a shallow to sub-vertical dip towards the NW, and C surfaces carry a mineral elongation lineation that plunges to the NE. The deformation patterns provide evidence for a sinistral, transpressive setting with a top-to-the-south directed motion (Fig. 3e). The strike-slip component of the finite deformation that is well expressed in the greenschist facies mylonites of the Murchison Unit is not observed in the Silwana Amphibolites.

2.3.2. The "La France Fault"

The La France Formation is separated from the greenschist-facies rocks of the Murchison Unit by a highly deformed zone a few dozen metres wide, hereafter named the "La France Fault". The lithologies in contact with the northern boundary of the La France Formation range from talc schists and serpentinites to chlorite schists containing primary carbonates. Within the shear zone, the schists display open to tight folds with decimetric wavelengths. At least two sets of such folds are found, with axes displaying shallow plunges of 5 - 10° to the NW and SW respectively. Unfortunately, poor outcrop conditions restricted to exploration trenches, among other constraints, prevented a more extensive study of fold patterns. Mineral elongation lineations on shear-zone-parallel cleavages plunge preferentially to the NE, whereas shear sense indicators, such as mineral fish and asymmetric shadow zones around porphyroblasts, point to a top-to-the-south motion (Fig. 3f). These patterns in combination provide evidence for a sinistral component during a general top-to-the-south reverse faulting, similar to that observed along the Letaba Shear Zone. The latter interpretation is also in agreement with structures observed within the La France formation to the south of the shear zone. The La France schists exhibit recumbent folds axial planar to the metamorphic banding, and are affected by crenulations with shallow-plunging axes. These structures are illustrative of a shortening accommodated by reverse faulting.

To the south, the La France Formation is in contact with the 2795 ± 8 Ma Ma Lekkersmaak granite (Zeh et al. 2009) and with the 2820 ± 38 Ma Willie granite (Poujol, 2001), which form part of the Voster Suite. The granites contain micaschist xenoliths derived from the La France Formation. They are mostly undeformed except for occasional shear bands formed under sub-solidus conditions. The field relationships clearly indicate that the Lekkersmaak and Willie intrusions postdate the deformation and metamorphism in the La France Formation.

2.3.3. Other structures

The Antimony Line is a steeply north dipping mineralised shear zone within the Murchison Unit. The dominant fabric consists of isoclinal folds axial-planar to the metamorphic banding, along with S-C planes indicating a top-to-the-south motion. Mineral elongation lineations plunge vertically to moderately eastwards. These structures illustrate a general transpressive, sinistral setting in the Murchison Unit, accompanied by a significant reverse component (Vearncombe et al., 1988, 1992). They are consistent with the kinematics observed in the Letaba and La France shear zones. At a larger scale, they are in general agreement with the regional-scale sinistral transpressive regime and illustrate deformation localisation in the regional strain field, described in Jaguin et al. (2012).

3. Petrography, fabrics and mineral chemistry

A summary of the main petrographic and textural characteristics of the rocks sampled from the different formations of the MGB is presented in Table 1. Details of analytical techniques used to determine mineral chemistry are given in Appendix (A1).

3.1. La France Formation

Field observations and microstructural studies of quartzites and micaschists of the La France Formation provide evidence that a primary compositional layering S_0 was modified during an early D_1 deformation event, leading to the formation of a composite S_0/S_1 foliation. The S_0/S_1 foliation was subsequently affected by the main D_2 deformation event (Fig 4b, e). The latter caused the formation of the predominant S_2 fabric that is axial-planar to recumbent folds. The S_2 planes are mostly defined by quartz (Q) ribbons, biotite (Bt), and minor muscovite (Ms). They bear a L_2 mineral elongation lineation. In metapelitic layers syn-deformation staurolite (St), garnet (Gt) and kyanite (Ky) porphyroblasts can additionally be observed, although the latter two are not found together in the same sample (Fig. 4a and 4c). Plagioclase feldspar

(Pl) sillimanite (Sill) and cordierite (Crd) occasionally occur in the kyanite-bearing schists. The S_2 schistose planes were crenulated as a result of a D_3 deformation event, leading to the formation of kinks with a mm- to cm-scale wavelength, and of a crude S_3 cleavage. In kyanite-bearing micaschist, some kyanite, staurolite and chlorite were kinked during D_3 crenulation, while new chlorite, staurolite and muscovite develop in the kink axes (Fig. 4f). The final minerals thus form syn- to post-D_3 assemblages.

The garnet-bearing micaschists display the following peak assemblage:

(A): Gt + St + Bt_1 + Ms_1 + Q

In these rocks, syn-deformation garnet porphyroblasts with quartz inclusion trails are commonly overgrown by syn-deformation staurolite, with similarly oriented quartz inclusion trails, indicating the successive formation of both minerals during the deformation event D_2 (Fig. 4d). Hematite is always a retrograde phase, which formed along cracks in altered garnet grains, mostly at garnet rims. The peak metamorphic fabric is overgrown by post-deformation biotite (Bt_2) and muscovite (Ms_2). Garnet porphyroblasts show a continuous prograde growth zoning, characterised by increasing X_{Py} (Mg/(Mg+Fe+Ca+Mn)) from 0.05 to 0.09 and Mg# (Mg/(Fe+Mg)) from 0.07 to 0.09, and decreasing X_{Sps} (Mn/(Mg+Fe+Ca+Mn)) from 0.12-0.06 to 0.03 and X_{Grs} (Ca/(Mg+Fe+Ca+Mn)) from 0.07 to 0.06, all from core to rim. Staurolite has Mg# of 0.12-0.14. The Mg# of syn-D_2 biotite (Bt_1) ranges from 0.32 to 0.44 range, while post-D_2 biotite (Bt_2) has Mg# = 0.44, suggesting partial reequilibration of Bt_1. Muscovite (Ms_1 and Ms_2) has low Si of 3.05 a.pf.u. (atoms per formular unit) and a relatively high paragonite component, as is reflected by Na/(Na+K+Ca) = 0.17. Representative mineral compositions are shown in Table 2.

Kyanite-bearing schists (B) provide evidence for the successive formation of different equilibrium assemblages during peak and retrograde evolution. The peak metamorphic conditions are illustrated by

syn-D_2 kyanite porphyroblasts that commonly contain biotite, muscovite and quartz inclusions. Some rocks additionally bear syn-D_2 staurolite porphyroblasts, produced with kyanite, presumably during the progressive breakdown of chlorite (which completely reacted out). Thus the thin section observations indicate that the following assemblage formed during D_2 deformation at peak pressures (Fig. 4b):

(B1) $Ky_1 + Bt_1 + Pl + Ms_1 + Q \pm St_1$.

The occurrence of prismatic sillimanite, as well as of fibrolite around kyanite indicates that the kyanite-bearing schists crossed the phase transition Ky → Sill. The coexistence of sillimanite and cordierite (Crd) (Mg# = 0.75-0.77; Na= 0.11 a.p.f.u.), which together form patches about 0.5mm wide, shows furthermore that assemblage (B1) was later (partially) replaced by the assemblage:

(B2) $Sill + Bt_2 + Crd + Pl + Q$.

Subsequently, the cordierite grains were partially replaced by a new generation of micrometric staurolite grains, which are closely intergrown with fine grained, chlorite and symplectitic muscovite. These intergrowth relationships indicate that the final mineral assemblage in the kyanite-bearing schists was:

(B3) $St_3 + Bt_3 + Ms_3 + Chl + Q$.

Retrograde staurolite St_3 generally has higher Mg# of 0.19-0.24 than the prograde and peak metamorphic staurolite St_1, with Mg# of 0.13-0.20. In contrast, biotite from all the successive assemblages (Bt_1 to Bt_3) overlap in compositions, with Mg# = 0.62-0.64, Ti^{vi} = ~ 0.06. This is interpreted to be the result of widespread chemical reequilibration of biotite composition during metamorphic evolution. Prograde muscovite (Ms_1) always shows lower Na/(Na+K+Ca) of 0.08 and higher silica contents (Si = 3.15 a.p.f.u.) than retrograde muscovite (Ms_3), with Na/(Na+K+Ca) = 0.18 and Si= 3.02 a.p.f.u.. M.

/(Na+K+Ca) = 0.08. Retrograde chlorite of assemblage (B3) has Mg# = 0.66-0.69, and high-Al contents of 1.35 a.p.f.u. Plagioclase grains show a wide range of chemical compositions, with X_{An} (Ca/Ca+Na) = 0.09 to 0.41, and a majority of grains having X_{An} ~ 0.4.

In one sample from the same formation, centimetric euhedral kyanite (Ky_3) and staurolite (St_3) crystals overgrow the S_2 metamorphic banding, together with millimetric biotite and muscovite grains (Fig. 4e and 4f). This assemblage, equivalent to (B_3) in more aluminous lithologies, suggests that the Sill → Ky phase transition was crossed during the retrograde evolution of the rock. Furthermore, the retrograde assemblages (B_2) and (B_3) are characterised by the formation of abundant hydrated minerals, indicating a secondary, H_2O-rich fluid enrichment after peak metamorphism.

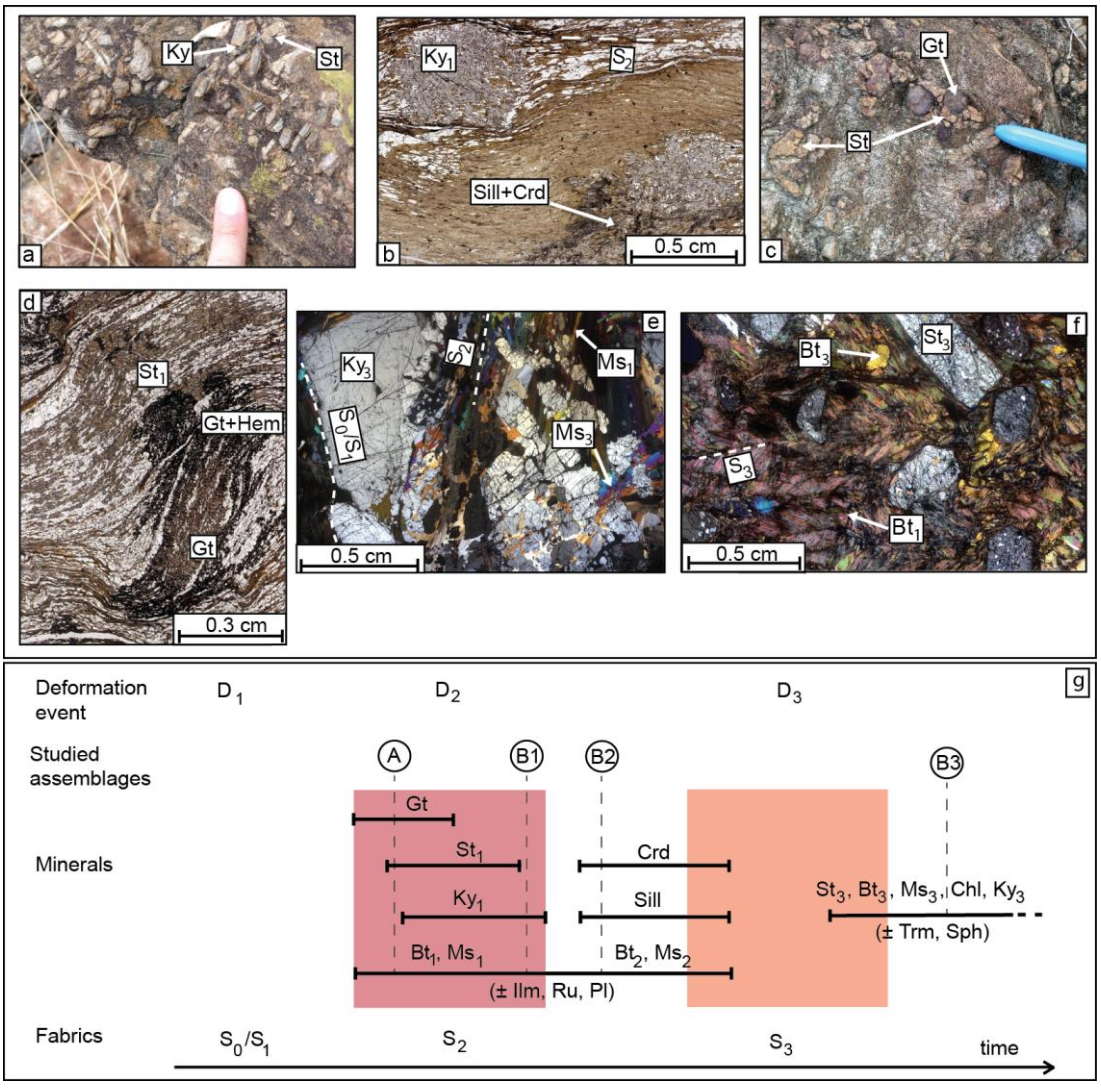

Figure 4:

Petrographic features observed in rocks of the La France formation. (a) Biotite micaschist with protruding staurolite (St) and kyanite (Ky) porphyroblasts. (b) Thin section of a kyanite- staurolite-

cordierite-bearing micaschist (sample B). Ky porphyroblasts are surrounded by foliation-parallel biotite and quartz (top), or are overgrown by patches of sillimanite and cordierite. (c) Garnet (Gt)- staurolite-bearing micaschist (sample A). (d) Thin section of sample A showing highly deformed and rotated St and Gt porphyroblasts (syn-D_2), set in a matrix of biotite, muscovite and quartz. Hematite (Hem) occurs along cracks mostly in garnet rims, probably resulting from retrograde alteration. Biotite and muscovite define the syn-D_2 metamorphic banding. (e) and (f) Thin sections of a Ky- St-bearing schist from the La France formation showing, (e) a compositional layering S_0/S_1 delimiting a kyanite and muscovite-rich layer, with Ky overgrowing the D_2 metamorphic fabric, (f) a crenulated domain, with euhedral staurolite and a crude S_3 cleavage. (g) Synopsis showing the relative temporal relationships between deformation and assemblage formation in the La France Formation (Ilm: Ilmenite, Ru : Rutile, Trm : Tourmaline, Sph : Sphene).

3.2. Silwana Amphibolites

The Silwana Amphibolites trend ENE – WSW and show a vertical to steeply north-dipping S_0/S_1 layering defined by modal variations of quartz, plagioclase and hornblende (Hbl) across bands about 10 cm thick. On a smaller scale, the amphibolites develop a planar (S > L), flattening tectonic fabric S_2. The metamorphic banding S_2, is subparallel to the S_0/S_1 layering. It is defined by the alternation of millimetric hornblende-rich and quartz- plagioclase-rich bands. The latter display an equigranular texture, suggesting a relatively high temperature recrystallisation (>500°C). The S_2 foliation bears a dominant steep easterly dipping mineral lineation L_2 defined by hornblende. At the north-western extremity of the sliver, the strike of the layering changes dramatically from ENE-WSW to NW–SE, with a steep north-easterly dip, while the S_2 foliation carries a steep, north-plunging mineral elongation lineation. It is likely that both the ENE- and NW-trending structures (and related lineations) result from activation of a conjugate shear system. Garnet occurs as an additional phase in rare Al- and Fe-rich layers. Biotite is also present in small proportions (~1-2 modal %). Epidote (Ep) is a retrograde phase and frequently formed in cross-cutting veins, in association with carbonates. Chlorite is found in cracks within garnet porphyroblasts The peak metamorphic assemblage is interpreted to be:

(S) Gt + Hbl + Pl + Bt + Ilm + Q.

The garnet prophyroblasts show a slight prograde growth zoning, as is reflected by increasing X_{Py} (from 0.055 to 0.060, Mg# varies from 0.67 to 0.73) and X_{Grs} (from 0.13 to 0.15), and decreasing X_{Sps} (from 0.04 to 0.03) and X_{Alm} (Fe/(Fe+Mg+Ca+Mn) from 0.77 to 0.76) from core to rim. Garnet contains inclusions of hornblende, quartz and ilmenite. Hornblende inclusions in garnet show some scatter in their chemical composition, with Mg# = 0.21–0.26 and Ca/Na = 3.0-3.6, compared to Mg# = 0.23-0.26 and Ca/Na = 2.8-3.0 for matrix hornblende. Matrix plagioclase has a constant chemical composition, with X_{An} = 0.17. Biotite occurrence is limited, with small grains elongated parallel to hornblende, and some randomly oriented grains occurring around garnet. All matrix biotites show similar compositions with Mg# = 0.22-0.26 and Ti^{vi} = 0.1 a.p.f.u.. Retrograde chlorite (Mg# = ~0.36) only formed along cracks in the garnet porphyroblasts.

3.3. Murchison Unit

Strain distribution in the Murchison Unit is fairly heterogeneous. Minor domains, far from tectonic discontinuities, are almost undeformed, but most rocks displays a pervasive schistose fabric and provide evidence for a poly-phased deformation (Vearncombe, 1988 ; Vearncombe et al., 1988, 1992 ; Jaguin et al., 2012). Primary sedimentary structures S_0, are only preserved in competent layers. Stratigraphic contacts between the different formations of the Murchison Unit have been completely reworked by tectonic processes during the successive deformation events. A first deformation episode D_1 corresponds to the formation isoclinal folds axial-planar to a S_1 cleavage trending ENE. These isoclinal folds are transposed by E-W trending, S-shaped asymmetric folds, axial planar to a S_2 cleavage, formed during a second deformation event, D_2. However, it is generally difficult to attribute the pervasive cleavages to either D_1 or D_2. None of our samples exhibit the D_3 crenulation cleavage, which was recognised by

Vearncombe et al. (1988, 1992) in rocks near to the Antimony Line. For P—T path estimates, we investigated a sample from a nearly undeformed metamafic rock from the centre of the Murchison Unit, south of the Antimony Line (sample M1); and a sample from a deformed quartzite with metapelitic layers from the southern edge of the Murchison Unit (sample M2), a few dozen metres north from the contact with the Makhutswi gneisses (Fig. 2). The metabasite sample M1 contains the following peak metamorphic mineral assemblage:

(M1) Act (actinolite) + Ab (albite) + Ep + Chl + Sph (sphene)

with Chl mostly in late shear bands. The actinolite needles display a garbenscheifer texture, which might represent pseudomorphs of primary magmatic textures, and have Mg# = 0.67-0.72. The feldspar is pure albite ($X_{An} \leq 0.01$). Chlorite has Mg# = 0.55-0.56 and Al^{vi} = 1.20 a.p.f.u..

The metapelitic-quartzitic sample M2 displays the following peak mineral assemblage:

(M2) Gt + Ms + Bt + Chl + Qtz,

and additionally contains retrograde chlorite along garnet cracks. Garnet porphyroblasts have diameters < 0.5mm and do not display any chemical zoning. The garnets have a high almandine components of X_{Alm} = 0.8, low pyrope and spessartine components ($X_{Py} = X_{Sps} = \sim 0.1$), and Mg# = 0.08-0.10. Biotite is Ti-poor (Ti^{vi}= 0.07 a.p.f.u.) and has a Mg# = 0.39-0.44. Chlorite has Mg# = 0.36-0.39 and Al^{vi} = 1.55-1.70 a.p.f.u. Muscovite is Na-poor, with Na/(Na+K+Ca) = 0.13, and Si= 3.1 a.p.f.u..

Table 2:
Major element compositions and structural formulae of representative mineral analyses of the peak and retrograde assemblages in lithologies from the La France Formation, Murchison Unit and Silwana Amphibolites.

Sample	A (garnet- staurolite micaschist of the La France Formation)									
Mineral phase	Gt (core)	Gt (core)	Gt(rim)	St (core)	St (rim)	Bt_1	Bt_1	Bt_2	Ms_1	Ms_2
wt%										
Na_2O				b.d.l.	b.d.l.	0.08	0.16	0.22	1.23	1.31
MgO	1.36	1.67	2.21	1.36	1.22	7.39	5.10	8.19	0.42	0.45
Al_2O_3	20.7	20.7	21.0	53.9	54.2	21.6	21.3	19.8	36.6	36.5
SiO_2	36.5	36.7	36.6	26.4	26.3	37.9	36.4	34.8	46.0	45.9
K_2O						7.22	7.50	6.61	9.22	9.46
CaO	2.65	2.07	1.95	b.d.l.	b.d.l.	0.14	0.16	0.08	0.01	0.04
TiO_2				0.22	0.34	0.98	0.65	0.95	0.09	0.07
Cr_2O_3						0.03	0.05	0.03	0.07	0.01
MnO	5.44	3.59	1.17	0.02	0.06	0.01	b.d.l.	b.d.l.	b.d.l.	0.01
FeO	34.2	35.0	37.6	15.7	15.1	16.8	19.4	18.4	1.16	1.04
Total	100.8	100.4	100.4	97.6	97.2	92.1	90.7	89.1	94.8	94.7
Oxygens	12	12	12	48	48	22	22	22	22	22
Si	5.93	5.97	5.93	7.42	7.41	5.76	5.73	5.54	6.11	6.11
Al^{IV}	0.07	0.03	0.07	0.58	0.59	2.24	2.27	2.46	1.89	1.89
Al^{VI}	3.94	3.98	3.90	17.3	17.4	1.70	1.59	1.26	3.84	3.83
Fe^{3+}	0.19	0.03	0.25	0.67	0.55					
Ti				0.05	0.07	0.10	0.11	0.11	0.01	0.01
Cr						0.00	0.00	0.00		
Mg	0.53	0.39	0.33	0.57	0.51	1.58	1.67	1.94	0.08	0.09
Fe^{2+}	4.90	4.87	4.39	3.03	3.00	2.10	2.12	2.45	0.13	0.12
Mn^{2+}	0.16	0.37	0.75	0.01	0.01	0.00				
Ca	0.34	0.39	0.46			0.07	0.02	0.01	0.00	0.01
Na						0.01	0.02	0.07	0.32	0.34
K						1.23	1.39	1.34	1.56	1.61
x[Py]	0.05	0.06	0.09							
x[Alm]	0.75	0.81	0.83							
x[Sps]	0.12	0.06	0.03							
x[Grs]	0.07	0.06	0.06							
xFe[fcel]									0.06	0.06
xMg[mcel]									0.04	0.04
xAl[mphen]									0.89	0.90

462

Sample	B (kyanite- plagioclase micaschist of the La France Formation)											
Mineral phase	Pl	Pl	St_3	St_3	Bt_1	Bt_3	Crd	Crd	Wm_1	Wm_3	Chl	Chl
wt%												
Na_2O	6.65	10.5			0.35	0.21	0.68	0.44	0.36	1.41	b.d.l.	0.03
MgO	0.01	0.02	1.98	2.17	13.26	14.40	9.56	9.68	2.76	1.19	18.8	19.4
Al_2O_3	26.9	21.2	54.1	53.9	19.4	19.2	32.6	32.8	33.1	36.8	22.9	22.7
SiO_2	57.3	66.1	28.9	29.1	36.5	35.2	49.1	49.0	46.6	46.0	25.5	26.0
K_2O	0.04	b.d.l.			9.12	8.40	0.01	0.02	6.02	9.28	0.44	0.68
CaO	8.45	1.99	b.d.l.	b.d.l.	0.04	0.04	0.07	0.03	0.42	0.02	0.10	0.05
TiO_2	0.01	b.d.l.	0.13	0.05	1.09	0.69	0.06	b.d.l.	0.00	0.04	0.02	0.05
Cr_2O_3			0.06	b.d.l.	0.24	0.14					0.05	0.37
MnO	0.01	0.02	0.48	0.42	0.08	0.13	0.19	0.12	0.01	0.02	0.16	0.11
FeO			12.3	12.2	13.9	15.3	5.57	5.41	2.79	1.06	17.3	16.4

Fe_2O_3	b.d.l.	0.06										
Total	99.4	99.8	98.0	97.8	94.0	93.7	97.9	97.4	92.0	95.9	85.2	85.8
Oxygens	32	32	48	48	22	22	18	18	22	22	28	28
Si	10.3	11.6	7.95	8.00	5.47	5.32	5.03	5.03	6.29	6.06	5.30	5.35
Al^{IV}	5.72	4.39	0.05		2.53	2.68	0.97	0.97	1.71	1.94	2.70	2.65
Al^{VI}			17.5	17.5	0.89	0.74	2.97	2.99	3.57	3.77	2.92	2.86
Fe^{3+}			0.49	0.53								
Ti			0.03	0.01	0.12	0.08						0.01
Cr			0.01		0.03	0.02					0.01	0.06
Mg			0.81	0.89	2.96	3.24	1.46	1.48	0.56	0.23	5.84	5.97
Fe^{2+}		0.01	2.34	2.27	1.74	1.94	0.48	0.46	0.32	0.12	3.01	2.82
Mn^{2+}			0.11	0.10	0.01	0.02	0.02	0.01			0.03	0.02
Ca	1.63	0.38			0.01	0.01	0.01		0.06		0.02	0.01
Na	2.32	3.57			0.10	0.06	0.14	0.09	0.10	0.36		0.01
K	0.01				1.74	1.62			1.04	1.56	0.12	0.18
xK [Or]	0.00	0.01										
xNa [Ab]	0.59	0.90										
xCa [An]	0.41	0.09										
xFe[fcel]									0.14	0.06		
xMg[mcel]									0.25	0.11		
Al[mphen]									0.61	0.83		

Sample	M1 (greenstone from the Murchison Unit)							
Mineral phase	Act	Act	Chl	Chl	Pl	Pl	Ep	Sph
wt%								
Na_2O					11.7	11.9		
MgO	19.6	19.0	21.5	22.7				
Al_2O_3	1.02	0.96	20.1	20.5	19.6	19.9	21.9	0.69
SiO_2	56.2	55.3	27.5	27.9	67.5	67.4	36.8	30.6
K_2O					b.d.l.	b.d.l.		
CaO	13.0	13.1			0.12	0.20	23.13	29.0
TiO_2	b.d.l.	0.16	b.d.l.	0.16				37.9
Cr_2O_3	0.52	0.18	0.34	0.21				0.26
MnO	0.26	0.23	0.23	0.19				
FeO	8.53	9.70	17.58	17.92				0.41
Fe_2O_3					b.d.l.	0.30	15.0	
Total	99.1	98.6	87.2	89.6	98.8	99.7	96.8	98.8
Oxygens	23	23	28	28	32	32	13	5
Si	7.82	7.79	5.59	5.52	11.9	11.9	3.10	1.01
Al^{IV}	0.17	0.16	2.41	2.48	4.08	4.12		0.03
Al^{VI}			2.39	2.30			2.17	
Fe^{3+}						0.03	0.95	0.01
Ti		0.02		0.02				0.94
Cr	0.06	0.02	0.05	0.03				0.01
Mg	4.06	3.98	6.51	6.69				
Fe^{2+}	0.99	1.14	2.99	2.97		0.01	0.01	
Mn^{2+}	0.03	0.03	0.04	0.03				
Ca	1.94	1.97			0.02	0.04		1.02
Na					4.00	4.04		
K								
xK [Or]								
xNa [Ab]					0.99	0.99		
xCa [An]					0.01	0.01		
x[cZo] = x[Zo]							0.09	

x[Ep]	0.91
x[Pie]	0.00

464

Sample	M2 (garnet- bearing aluminous quartzite of the Murchison Unit)							
Mineral phase	Gt	Gt	Bt	Bt	Chl	Chl	Wm	Wm
wt%								
Na_2O			0.07	0.09	0.04	0.03	0.93	1.06
MgO	2.31	1.80	7.12	7.99	8.85	8.65	0.73	0.81
Al_2O_3	20.9	20.7	16.7	18.0	19.2	18.2	35.7	35.3
SiO_2	36.7	36.4	39.8	36.6	30.0	32.7	46.5	46.6
K_2O			6.77	6.53	1.61	1.62	9.66	9.88
CaO	0.41	0.75	0.78	0.41	0.55	0.69	0.05	0.02
TiO_2			1.16	1.31	0.08	0.04	0.18	0.34
Cr_2O_3			0.15	0.12	0.10	b.d.l.	b.d.l.	0.21
MnO	4.63	6.06	0.16	0.13	0.23	0.32	0.01	0.02
FeO	35.5	34.6	19.9	18.4	27.7	23.5	1.4	1.2
Total	100.4	100.3	92.6	89.6	88.4	85.8	95.1	95.3
Oxygens	12	12	22	22	28	28	22	22
Si	5.95	5.95	6.10	5.79	6.34	6.92	6.17	6.18
Al^{IV}	0.05	0.05	1.90	2.21	1.66	1.08	1.83	1.82
Al^{VI}	3.96	3.93	1.11	1.13	3.13	3.46	3.76	3.70
Fe^{3+}	0.13	0.19						
Ti			0.13	0.16	0.01	0.01	0.02	0.03
Cr			0.02	0.02	0.02			0.02
Mg	0.56	0.44	1.63	1.88	2.79	2.73	0.14	0.16
Fe^{2+}	4.69	4.54	2.54	2.43	4.90	4.16	0.15	0.13
Mn^{2+}	0.64	0.84	0.02	0.02	0.04	0.06		
Ca	0.07	0.13	0.13	0.07	0.12	0.16	0.01	
Na			0.02	0.03	0.02	0.01	0.24	0.27
K			1.32	1.32	0.44	0.44	1.64	1.67
x[Py]	0.09	0.07						
x[Alm]	0.79	0.77						
x[Sps]	0.10	0.14						
x[Grs]	0.01	0.02						
xFe[fcel]							0.08	0.07
xMg[mcel]							0.07	0.08
xAl[mphen]							0.85	0.85

465

Sample	S (garnet- plagioclase- hornblende amphibolite from the Silwana Amphibolites)										
Mineral phase	Gt (core)	Gt (rim)	Hbl	Hbl in Gt	Bt	Bt	Pl	Pl	Ilm	Chl	Chl
wt%											
Na_2O			2.06	1.67	0.04	0.09	9.69	9.42		0.10	0.09
MgO	1.41	1.54	4.95	3.99	6.00	5.39			0.03	9.98	9.17
Al_2O_3	20.6	20.5	14.0	13.3	16.0	16.3	22.3	22.7	0.00	19.7	14.2
SiO_2	36.9	36.6	40.0	40.2	31.9	31.1	64.5	64.5		25.2	29.5
K_2O			0.56	0.41	6.63	5.23	0.04	0.08		0.13	1.85
CaO	4.94	5.26	10.4	11.0	0.02	0.14	3.55	3.58		0.13	0.24
TiO_2			0.60	0.27	1.90	1.60			52.3	0.63	1.62
MnO	1.97	1.52	0.10	0.15	0.08	0.04	b.d.l.	b.d.l.	0.49	0.06	0.04
FeO	34.9	34.7	24.8	26.2	30.3	33.6			46.9	31.4	30.2
Fe_2O_3							0.08	0.11			

Total	100.7	100.1	97.5	97.2	92.9	93.5	100.1	100.5	99.8	87.3	86.9
Oxygens	12	12	23	23	22	22	32	32	3	28	28
Si	5.97	5.95	6.25	6.3	5.26	5.14	11.4	11.3		5.52	6.50
Al^{IV}	0.03	0.05	1.75	1.67	2.74	2.86	4.63	4.70		2.48	1.50
Al^{VI}	3.89	3.87	0.82	0.80	0.36	0.31				2.62	2.19
Fe^{3+}	0.21	0.27					0.01		0.01		
Ti			0.07	0.03	0.24	0.20			1.00	0.10	0.27
Mg	0.34	0.37	1.15	0.94	1.47	1.33				3.26	3.01
Fe^{2+}	4.50	4.45	3.23	3.46	4.17	4.64		0.01	0.99	5.76	5.57
Mn^{2+}	0.27	0.21	0.01	0.02	0.01	0.01			0.01	0.01	0.01
Ca	0.86	0.92	1.74	1.86		0.02	0.67	0.67		0.03	0.06
Na			0.62	0.51	0.01	0.03	3.31	3.21		0.04	0.04
K			0.11	0.08	1.39	1.10	0.01	0.02		0.04	0.52
x[Py]	0.06	0.06									
x[Alm]	0.76	0.76									
x[Sps]	0.04	0.03									
x[Grs]	0.14	0.15									
xK [Or]							0.00	0.00			
xNa [Ab]							0.83	0.82			
xCa [An]							0.17	0.17			
xMg [Geik]									0.00		
xFe [Ilme]									0.99		
xMn [Pyro]									0.01		

4. Metamorphic P—T paths

P—T paths for the different units were inferred by comparison between the observed mineral assemblages, mineral compositions and zoning patterns, and those obtained by P—T pseudosection calculations for the respective samples. This methodology provides robust results, as has been shown by many examples in the past; for example see Zeh et al. (2001, 2004); Millonig et al. (2008, 2010). The methods used to estimate the effective bulk rock composition and to construct P—T pseudosections are described in the Appendix (A2).

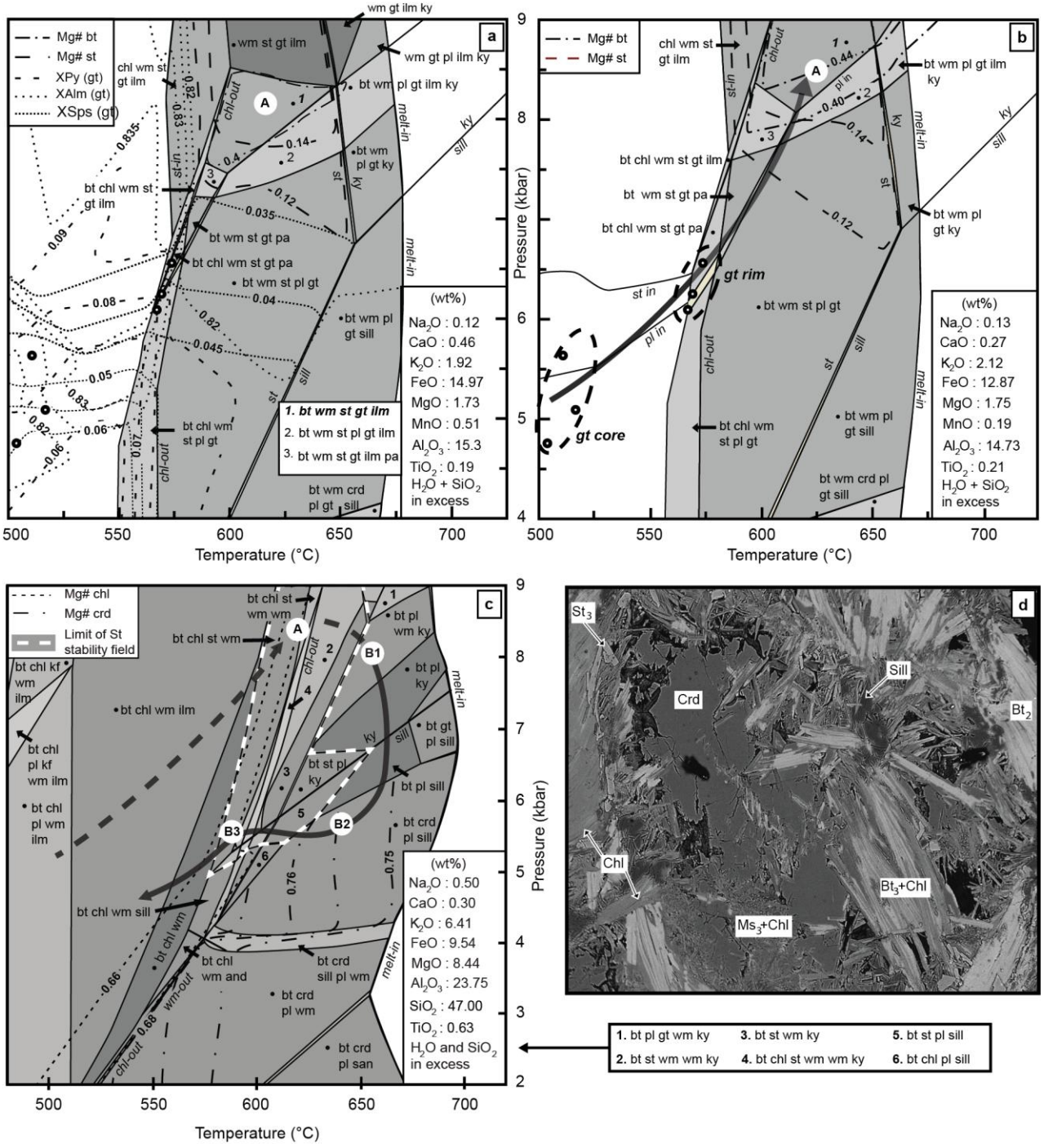

Figure 5:

P – T pseudosections for metapelitic rocks from the La France Formation, constructed in the model system (Mn)TiNCKFMASH (with H_2O and SiO_2 in excess). (a, b) P—T pseudosection for a garnet-staurolite micaschist (sample A) and (c) for a kyanite-bearing micaschist with retrograde cordierite and staurolite (sample B). The P—T pseudosection (a) is constructed by using the unfractionated bulk composition obtained by XRF analysis, and (b) is built by using the effective bulk composition after garnet growth ceased. Small open circles represent fit between calculated and measured garnet compositions, obtained from garnet cores and rims of zoned garnet in sample A. White circles labelled A, B1, B2, B3 mark the fields with the best agreement between observed and calculated mineral assemblages

and mineral compositions. The arrows define the P—T path inferred from the petrological constraints. (d) SEM image of sample B showing tiny staurolite grains (St_3), which together with chlorite (Chl), biotite (Bt_3) and muscovite (Ms_3) surround a cordierite (Crd) porphyroblast, intergrown with sillimanite (Sill) and biotite (Bt_2). Wm = white mica.

4.1. La France Formation

P—T pseudosections for the La France Formation were calculated for a Gt-St-bearing schist (sample A) and a Ky-St-Crd schist (sample B), which were collected about 300m apart. In the absence of any tectonic break between the two outcrops we assume that both rocks underwent the same metamorphic history, and consequently, that the different mineral assemblages and compositions result from different bulk rock compositions. Thus a detailed P—T path can be constructed by superimposing the information obtained from the different rock samples (e.g. Zeh et al., 2001, 2004; Reno et al. 2009).

Results of P—T pseudosections for sample A (Fig 5a, b) indicate that the Gt-St-bearing schists of the La France Formation experienced a prograde P—T increase from about 5.5 kbar, 520 °C to 7.5-9.0 kbar, 590-650 °C. The prograde P—T evolution is constrained by the agreement between observed and calculated garnet zoning patterns, using the "garnet isopleths intercept method" (e.g., Evans 2004; Zeh et al., 2006). The peak P—T conditions are determined from the correspondence between the calculated and observed peak mineral assemblage (A): Grt + St + Bt_1 + Ms_1 + Q, and related mineral compositions. It should be noted, however, that the fit between calculated and observed peak mineral compositions is not perfect, i.e. the calculated mineral compositions of garnet rims plot outside the phase field for the peak mineral assemblage (Fig. 5). This discrepancy may be explained by at least two reasons. Firstly, minerals in sample A underwent a retrograde equilibration (causing a change of the peak mineral composition of garnet rims and of biotites; e.g. Florence & Spear, 1991), and/or secondly, by internal fractionation, causing a change of the effective bulk composition during prograde garnet growth (e.g. Stüwe, 1997; Marmo et al., 2002; Zeh et al., 2006). The effects of chemical fractionation due to garnet growth are

modelled in Fig 5. Assemblage (A) is shifted from 7.5-8.5 kbar , 590-645°C for the unfractionated rock (Fig. 5a) to higher P—T conditions of 8.0-9.0 kbar , 600-650°C when fractionation is taken into account (Fig. 5b).

The peak metamorphic assemblage (B1) Ky_1 + Bt_1 + Pl + Ms_1 + Q ± St_1 observed in sample B requires peak P—T conditions of 6.8-9.0 kbar at 630–650°C. Comparison of the peak metamorphic conditions for sample B and the prograde P—T vector inferred for sample A indicates that the formation underwent a limited heating after reaching peak pressure. Syn-D2 muscovite in sample B has a modal proportion < 1%, suggesting equilibration near the white mica-out reaction curve that limits the multivarient field at lower pressures. Sillimanite overgrowth around kyanite and the finding of cordierite in assemblage (B2): Sill + Bt_2 + Crd + Pl + Q, provide evidence for a nearly isothermal decompression to P—T conditions of <6 kbar at 600-660°C during retrograde evolution (Fig. 5c.). Cordierite is partly replaced by an assemblage including St, Sill, Bt, Ms and Chl (assemblage (B3): St_3 + Bt_3 + Chl + Ms_3 + Q, Fig. 5d.), implying that the near isothermal decompression was followed by a near-isobaric cooling to <600°C at ~5.5 kbar. The change in the P—T path from a near-isothermal decompression to a near-isobaric cooling may correspond to the onset of the D_3 deformation event.

4.2. Silwana Amphibolites

Results of P—T pseudosection calculations indicate that the observed peak metamorphic assemblage (S): Gt + Hbl + Pl + Bt + Ilm + Q is stable over a wide P—T range at temperatures between 540 and 690°C and pressures between 4.6 and >11 kbar (Fig. 6). A prograde P—T path is inferred by comparing the observed and calculated mineral composition of garnet (cores and rims), amphibole inclusions in garnet and matrix amphibole, as well as of matrix plagioclase. Intersecting the isopleths for these minerals provides evidence for a P—T increase from ~4.5 kbar, 540 °C, to peak metamorphic conditions of 8.7-10 kbar at 630-670°C.

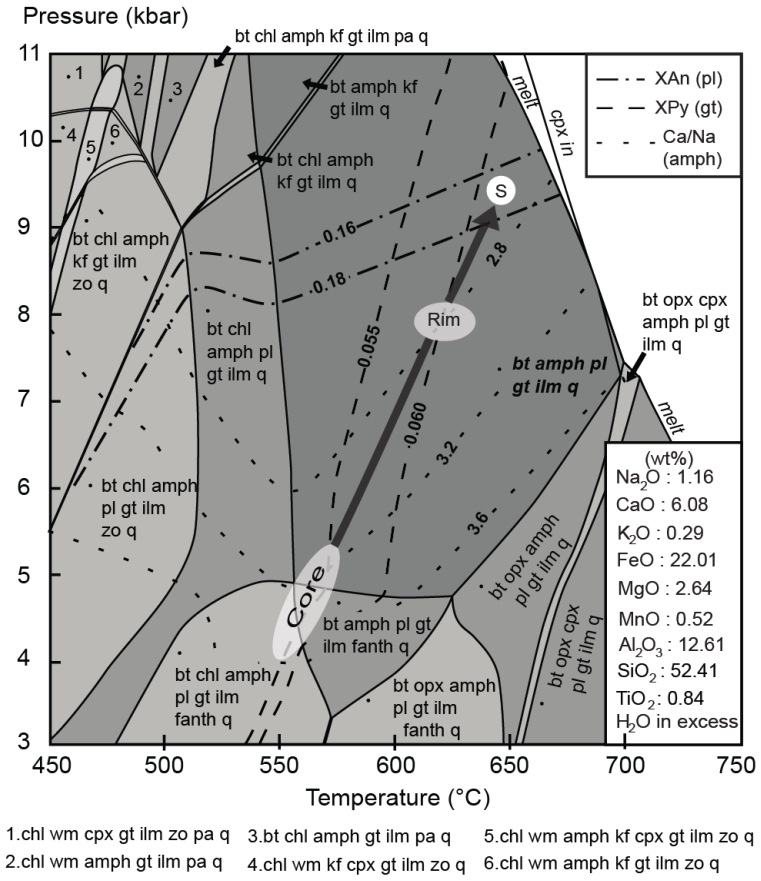

Figure 6:

P – T pseudosections for the Silwana Amphibolites. The pseudosection is constructed in the model system TiNCKFMASH system, with water in excess. White circles and ellipses mark the fields with the best agreement between observed and calculated assemblages and mineral compositions (core, rim, S). The multivariant field designated in bold-italics correspond to the observed peak assemblage. The arrows define the P—T vector inferred from petrological constraints. fanth = ferro-anthophyllite, pa = paragonite, zo = zoisite.

4.3. Murchison Unit

The model multivariant field corresponding to the metamorphic assemblage of sample M1: Act + Chl + Ab + Ep + Sph + Q (Fig. 7a) constrains metamorphic P—T conditions of 340-370°C at a wide pressure range from 1.3 to 5.8 kbar. The agreement between the measured and calculated actinolite composition restricts the metamorphic pressure conditions to 1.3-2.8 kbar at 340-370 °C (hatched field in Fig. 7a). However, it should be noted that clinozoisite (cz) instead of epidote has been calculated, due to the fact that the Fe^{3+} content was approximated to be 0 during the calculations (see Appendix A2). The observed

Mg# of chlorite falls in a P—T space characterised by even lower temperatures of 240 – 300°C (not shown). The latter may be indicative of chlorite (which is present in late-stage shear bands) crystallisation and/or re-equilibration during retrograde cooling. In summary, the geobarometric constraints for sample M1 point to a lower greenschist-facies metamorphism.

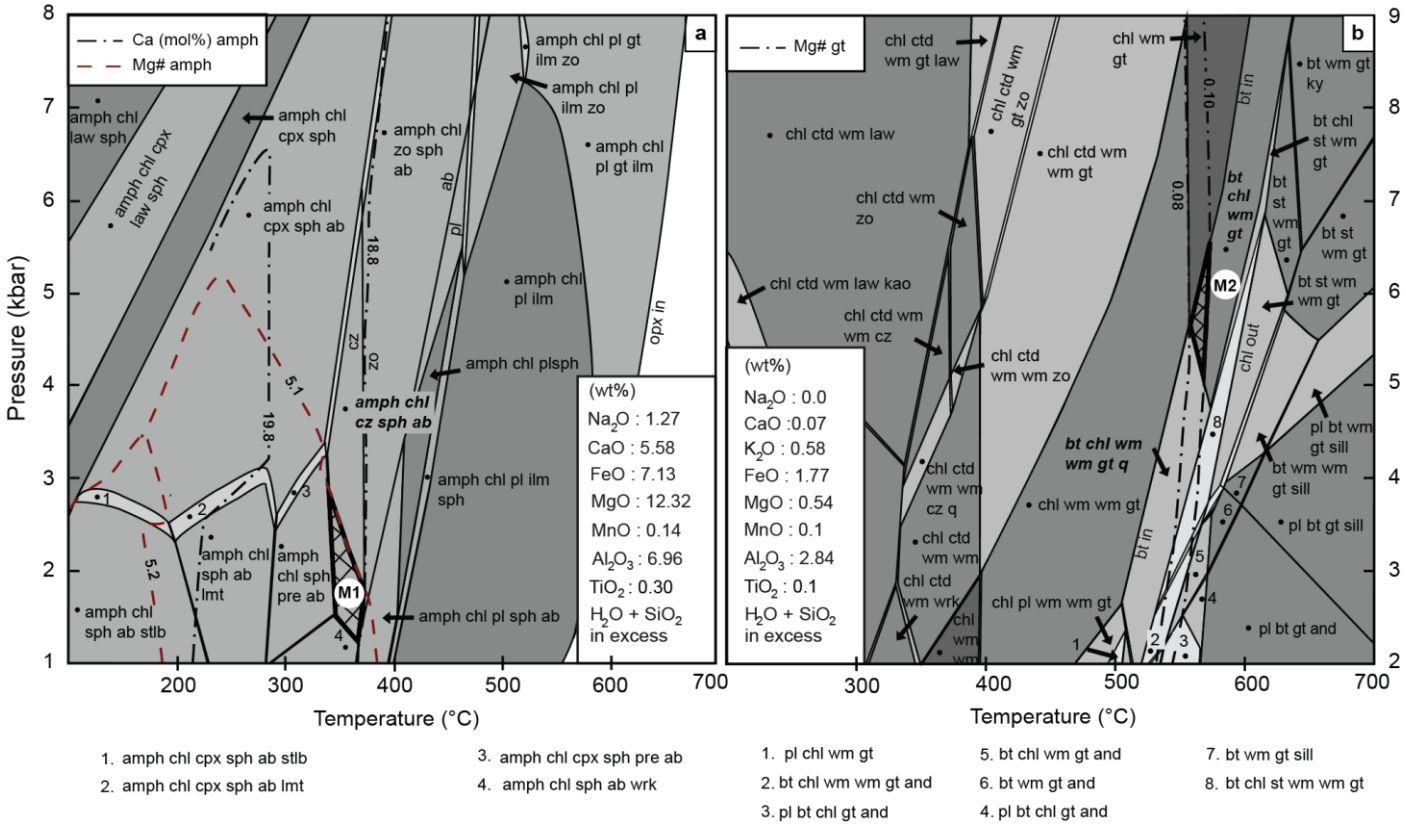

Figure 7:

P – T pseudosections for rocks from the Murchison Unit. (a) Metabasite from the center of the Murchison unit, sample M1. (b) Garnet-bearing aluminous quartzite from the southern edge of the Murchison Unit. Hatched areas labelled M1 and M2 mark the fields with the best agreement between observed and calculated assemblages and mineral compositions. Wm = white mica, and = andalusite, zo =zoisite, cz = clinozoisite, ab = albite, pre = prehnite, wrk = wairakite, lmt = laumontite, stlb = stilbite, kao = kaolinite.

The P—T pseudosection constructed for the metapelite sample M2, containing the peak metamorphic assemblage (M2) Gt + Ms + Bt + Chl + Qtz , indicates peak temperatures between 530 and 570 °C, at pressures between 5.0 and 6.2 kbar (hatched phase field in Fig. 7b). The peak metamorphic temperature conditions are constrained by two temperature-dependant field boundaries, the biotite-in and

chlorite-out / staurolite-in phase boundaries, as well as by the the fit between modelled and measured Mg# of garnet (Fig. 7b). The finding of muscovite without other white micas in sample M2 furthermore requires peak pressure conditions between 5.0 and 6.2 kbars at 550-570°C. The metamorphic grade of sample M2 is somewhat higher than that of sample M1, at the transition between high T greenschist and low P amphibolite facies, but is significantly lower than that of the rocks from the La France Formation and Silwana Amphibolites.

5. Geochronology

In order to constrain the timing of metamorphism and deformation in the MGB, LA-ICP-MS U-Pb dating was carried out on a syn-deformation granite intrusive in the Letaba Shear Zone (sample mur0982, see Fig. 2 for location). In addition, monazite and xenotime from the kyanite-bearing metapelite from the La France Formation (sample B) were dated.

The zircon grains were characterised by cathololuminescence imaging prior to analyses and were analysed on grain mounts, while monazite and xenotime U-Pb analyses were carried out on a thin section, after their characterisation by back-scattered electron imaging. The results are shown in Table 3 and in Fig. 8. Analytical techniques and data processing methods are detailed in Appendix (A3).

5.1 Zircons from magmatic rocks

Twenty zircons from the syn-deformation granite sample mur0982 intrusive into the LSZ to the North of the belt, displaying an oscillatory magmatic zoning, were analysed. Nineteen out of twenty U-Pb analyses plot along a discordia with an upper intercept at 2964 ± 5 Ma (MSWD = 5.4), whereas a xenocryst zircon

grain (28110411d) yields a much older $^{207}Pb/^{206}Pb$ age of 3251 ± 18 Ma (Table3). The upper intercept age is within error identical to a Concordia age (as of Ludwig, 1998) of 2964 ± 8 Ma (MSWD = 0.24, probability of concordance = 0.63, n=6) (Fig. 8a, b). It is interpreted to reflect the timing of the syn-tectonic granite emplacement. This interpretation is supported by the observation that the granite is intrusive in the Letaba Shear Zone and shows a mylonitic foliation that is coplanar with the mylonitic fabric of the greenschist-facies schists of the LSZ.

Table 3:

Top: U-Pb isotopic data obtained by LA-ICP-MS analyses carried out in GUF, and calculated ages from monazite and xenotime from sample B. Bottom: U-Pb isotopic data obtained by LA-ICP-MS analyses carried out in Clermont-Ferrand and calculated ages from zircons from sample mur0982.

Results of U-Pb LA-ICP-MS analyses of monazite (mnz) and xenotime (xno) carried out at Goethe University Frankfurt

sample		^{207}Pb[a] (cps)	U[b] (ppm)	Pb[b] (ppm)	Th[b]/U	^{206}Pb[c] (%)	^{206}Pb[d]/^{238}U	±2σ (%)	^{207}Pb[d]/^{235}U	±2σ (%)	^{207}Pb[d]/^{206}Pb	±2σ (%)	rho[e]	^{206}Pb/^{238}U	±2σ (Ma)	^{207}Pb/^{235}U	±2σ (Ma)	^{207}Pb/^{206}Pb	±2σ (Ma)	conc.[f] (%)
a04	mnz	253119	847	2900	21.1	0.57	0.4804	4.1	12.54	4.1	0.1894	0.5	0.99	2529	86	2646	39	2737	8	92
a05	mnz	536981	3062	6600	11.8	0.12	0.5312	2.0	14.00	2.1	0.1912	0.7	0.95	2747	45	2750	20	2752	11	100
a06	mnz	370826	2627	4100	7.7	1.07	0.4852	2.6	12.77	2.8	0.1909	1.0	0.93	2550	55	2663	27	2750	17	93
a07	mnz	519077	3342	5800	8.6	0.10	0.5504	2.4	14.53	2.5	0.1915	0.8	0.95	2827	54	2785	24	2755	12	103
a1core	xno	1149852	4946	3100	0.4	0.08	0.5562	8.1	16.11	8.2	0.2101	1.6	0.98	2851	189	2883	82	2906	26	98
a10	xno	1255656	4462	2700	0.4	0.09	0.5249	4.4	14.71	4.8	0.2033	1.9	0.92	2720	98	2797	46	2853	30	95
a12	mnz	630276	4092	8000	9.9	0.10	0.5122	2.1	13.43	2.2	0.1901	0.5	0.97	2666	46	2710	21	2743	9	97
a13	mnz	105973	403	1300	19.7	1.73	0.3219	13.4	8.25	13.5	0.1860	1.3	1.00	1799	214	2259	130	2707	21	66
a14	mnz	445663	4136	7900	8.9	0.08	0.5231	2.8	13.85	2.9	0.1921	0.7	0.97	2712	63	2740	28	2760	12	98
a15	mnz	404074	2226	5300	13.9	0.19	0.5245	2.1	13.71	2.2	0.1896	0.5	0.97	2718	47	2730	21	2739	9	99
a16	mnz	382514	2406	4800	10.6	0.43	0.5344	2.1	14.09	2.2	0.1912	0.7	0.95	2760	48	2756	21	2753	11	100
a19	mnz	448130	2403	6000	13.8	0.35	0.5410	2.4	14.24	2.7	0.1909	1.1	0.91	2788	55	2766	26	2750	18	101
a20	xno	1314118	6201	3500	0.2	0.05	0.5305	1.9	14.00	2.0	0.1915	0.5	0.96	2743	42	2750	19	2755	9	100
a21	mnz	118475	661	2200	24.6	0.92	0.4411	5.5	11.26	5.9	0.1851	2.1	0.94	2356	110	2545	57	2699	34	87
a22	mnz	268818	2076	5100	13.5	0.13	0.5268	3.7	13.91	3.7	0.1916	0.4	0.99	2728	82	2744	35	2756	7	99
a23	mnz	392774	2528	5200	11.1	0.11	0.5416	2.0	14.39	2.4	0.1928	1.2	0.86	2790	46	2776	23	2766	20	101
a25core	mnz	897089	3654	10000	17.4	0.10	0.5697	2.0	16.67	2.1	0.2122	0.7	0.95	2906	48	2916	21	2923	11	99
a25rim	mnz	509831	2393	6200	14.6	0.10	0.5254	1.8	13.86	2.0	0.1913	0.7	0.94	2722	41	2740	19	2754	11	99
a26	mnz	161910	845	1600	9.3	0.74	0.4560	6.2	12.09	6.4	0.1922	1.4	0.98	2422	127	2611	62	2761	23	88
a27	mnz	358562	2024	4900	14.3	0.10	0.5352	1.6	13.95	1.7	0.1890	0.4	0.97	2763	36	2746	16	2734	6	101
a28	mnz	381917	2499	5700	12.2	0.39	0.4678	3.0	12.18	3.1	0.1888	0.8	0.96	2474	62	2618	30	2732	14	91
a29	mnz	585399	3991	8300	10.5	0.24	0.5010	2.4	13.48	2.5	0.1952	0.8	0.94	2618	52	2714	24	2786	14	94
a30	xno	1764628	8893	5200	0.3	0.03	0.5292	1.8	14.04	1.8	0.1924	0.5	0.96	2738	39	2752	18	2763	9	99
a31	xno	1374114	8166	4700	0.2	0.03	0.5338	2.5	14.20	2.6	0.1929	0.7	0.96	2757	57	2763	25	2767	12	100
a32	mnz	52970	149	550	20.0	0.66	0.5146	6.3	13.27	6.3	0.1870	0.9	0.99	2676	139	2699	62	2716	15	99
a33	mnz	415719	2602	5100	10.7	1.14	0.5317	2.4	13.92	2.5	0.1899	0.8	0.95	2748	54	2744	24	2741	13	100
a34	mnz	519221	2744	6700	13.9	0.06	0.5319	2.4	14.02	2.5	0.1912	0.6	0.97	2749	54	2751	24	2753	10	100
a35	mnz	174257	741	2800	24.4	0.92	0.4369	3.7	11.37	3.9	0.1888	1.0	0.97	2337	73	2554	37	2732	16	86

a36	mnz	286783	1597	4100	15.4	0.13	0.5326	2.4	14.01	2.5	0.1907	0.6	0.97	2753	54	2750	24	2749	9	100

[a] Within run background-corrected mean ^{207}Pb signal in cps (counts per second).

[b] U and Pb content and Th/U ratio were calculated relative to GJ-1 reference zircon.

[c] percentage of the common Pb on the ^{206}Pb. b.d. = below dectection limit.
[d] corrected for background, within-run Pb/U fractionation (in case of $^{206}Pb/^{238}U$) and common Pb using Stacy and Kramers (1975) model Pb composition and subsequently normalised to GJ-1 (ID-TIMS value/measured value); $^{207}Pb/^{235}U$ calculated using $^{207}Pb/^{206}Pb/(^{238}U/^{206}Pb*1/137.88)$

[e] rho is the $^{206}Pb/^{238}U/^{207}Pb/^{235}U$ error correlation coefficient.

[f] degree of concordance = $^{206}Pb/^{238}U$ age / $^{207}Pb/^{206}Pb$ age x 100

611

Results of U-Pb LA-ICP-MS analyses of sample mur0982 carried out in Clermont Ferrand

		^{207}Pb[a] (cps)	U[b] (ppm)	Pb[c] (ppm)	Th[b] U	^{206}Pb[d] ^{238}U	±2σ (%)	^{207}Pb[d] ^{235}U	±2σ (%)	^{207}Pb[d] ^{206}Pb	±2σ (%)	rho[e]	^{206}Pb ^{238}U	±2σ (Ma)	^{207}Pb ^{235}U	±2σ (Ma)	^{207}Pb ^{206}Pb	±2σ (Ma)	conc.[f] (%)
mur0982																			
05	110411d	zr	8180	39	23	0.20	0.5956	2.0	17.74	2.1	0.2161	2.2	0.94	3012	48	2976	21	2952	35	102
06	110411d	zr	42538	408	126	0.38	0.3051	2.0	8.85	2.0	0.2103	2.1	0.97	1717	30	2323	18	2908	33	59
07	110411d	zr	16914	98	47	0.24	0.4921	2.0	14.69	2.1	0.2165	2.1	0.96	2580	42	2796	20	2955	34	87
08	110411d	zr	13025	73	35	0.20	0.5011	2.0	15.17	2.2	0.2195	2.3	0.92	2619	44	2826	21	2977	36	88
09	110411d	zr	55162	669	157	0.47	0.2496	2.0	7.08	2.0	0.2058	2.1	0.97	1436	25	2122	18	2873	34	50
10	110411d	zr	11560	67	32	0.32	0.5004	2.0	14.98	2.1	0.2171	2.2	0.94	2615	43	2814	20	2959	35	88
11	110411d	zr	21853	318	70	0.53	0.2313	2.0	5.96	2.1	0.187	2.2	0.94	1341	24	1970	19	2716	36	49
12	110411d	zr	11361	54	32	0.20	0.6084	2.0	18.27	2.2	0.2177	2.3	0.92	3064	50	3004	21	2964	36	103
15	110411d	zr	15607	79	44	0.23	0.5785	2.0	17.42	2.1	0.2184	2.2	0.94	2943	48	2958	21	2969	35	99
16	110411d	zr	22058	142	63	0.35	0.4593	2.0	13.75	2.1	0.2171	2.1	0.95	2437	41	2733	20	2960	34	82
17	110411d	zr	20140	121	56	0.25	0.4916	2.0	14.82	2.1	0.2186	2.1	0.94	2578	43	2804	20	2971	34	87
18	110411d	zr	12592	91	36	0.29	0.4169	2.0	12.36	2.2	0.2151	2.2	0.93	2246	39	2633	21	2944	35	76
19	110411d	zr	14013	74	39	0.18	0.5605	2.0	16.91	2.2	0.2188	2.2	0.94	2869	47	2930	21	2972	35	97
20	110411d	zr	9774	85	28	0.73	0.3431	2.1	10.32	2.2	0.2182	2.3	0.92	1902	34	2464	21	2968	36	64
21	110411d	zr	9362	49	26	0.18	0.5792	2.1	17.40	2.2	0.2179	2.2	0.92	2945	49	2957	22	2966	36	99
22	110411d	zr	10061	87	29	0.22	0.3513	2.1	10.53	2.3	0.2175	2.2	0.92	1941	35	2483	21	2962	36	66
25	110411d	zr	12745	66	36	0.21	0.5848	2.1	17.65	2.3	0.2189	2.3	0.91	2968	49	2971	22	2972	36	100
26	110411d	zr	11260	59	32	0.22	0.5851	2.1	17.58	2.3	0.2179	2.3	0.91	2969	49	2967	22	2966	36	100
27	110411d	zr	8942	47	26	0.21	0.5872	2.1	17.52	2.4	0.2165	2.3	0.89	2978	50	2964	23	2955	37	101
28	110411d	zr	21485	105	55	0.35	0.5329	2.1	19.16	2.3	0.2607	2.3	0.91	2754	47	3050	22	3251	35	85
29	110411d	zr	25554	211	76	0.28	0.3868	2.1	11.33	2.3	0.2123	2.3	0.90	2108	38	2550	22	2924	37	72

[a] Within run background-corrected mean ^{207}Pb signal in cps (counts per second).

[b] U and Pb content and Th/U ratio were calculated relative to GJ-1 reference zircon.

[c] percentage of the common Pb on the ^{206}Pb. b.d. = below dectection limit.
[d] corrected for background, within-run Pb/U fractionation (in case of $^{206}Pb/^{238}U$) and common Pb using Stacy and Kramers (1975) model Pb composition and subsequently normalised to GJ-1 (ID-TIMS value/measured value); $^{207}Pb/^{235}U$ calculated using $^{207}Pb/^{206}Pb/(^{238}U/^{206}Pb*1/137.88)$

[e] rho is the $^{206}Pb/^{238}U/^{207}Pb/^{235}U$ error correlation coefficient.

[f] degree of concordance = $^{206}Pb/^{238}U$ age / $^{207}Pb/^{206}Pb$ age x 100

612

613 ***5.2 Monazite and xenotime dating***

614

615 A total of 31 U-Th-Pb laser spot analyses were carried out on 18 monazite and 3 xenotime grains found in

616 the La France micaschists, sample B. The grains yielded two sets of concordant ages (Fig. 8c). Most

grains, which are intergrown with the matrix micas, yielded a concordant U-Pb age of 2752 ± 7 Ma. Xenotime and a monazite inclusions in kyanite porphyroblasts yielded much older concordant U-Pb ages of 2906 ± 26 and 2923 ± 11 Ma, respectively (grey ellipses in Fig. 8c). The stepwise decrease of the time resolved, common Pb corrected $^{207}Pb/^{206}Pb$ signal during the analysis of the monazite inclusion in kyanite indicated that this grain was zoned. The drop of $^{207}Pb/^{206}Pb$ signal corresponds to an age decrease from 2923 ± 11 Ma to 2754 ± 11 Ma (Fig. 8f). A possible explanation to this result is that kyanite and monazite formed at ca. 2923 Ma or prior to it, and that the monazite inclusion in kyanite subsequently underwent partial alteration and resetting at ca. 2754 Ma, simultaneous to the formation or complete re-crystallisation of matrix monazite and xenotime. We therefore suggest that the ca. 2923 Ma age represents a minimal age for the metamorphic peak in the La France Formation.

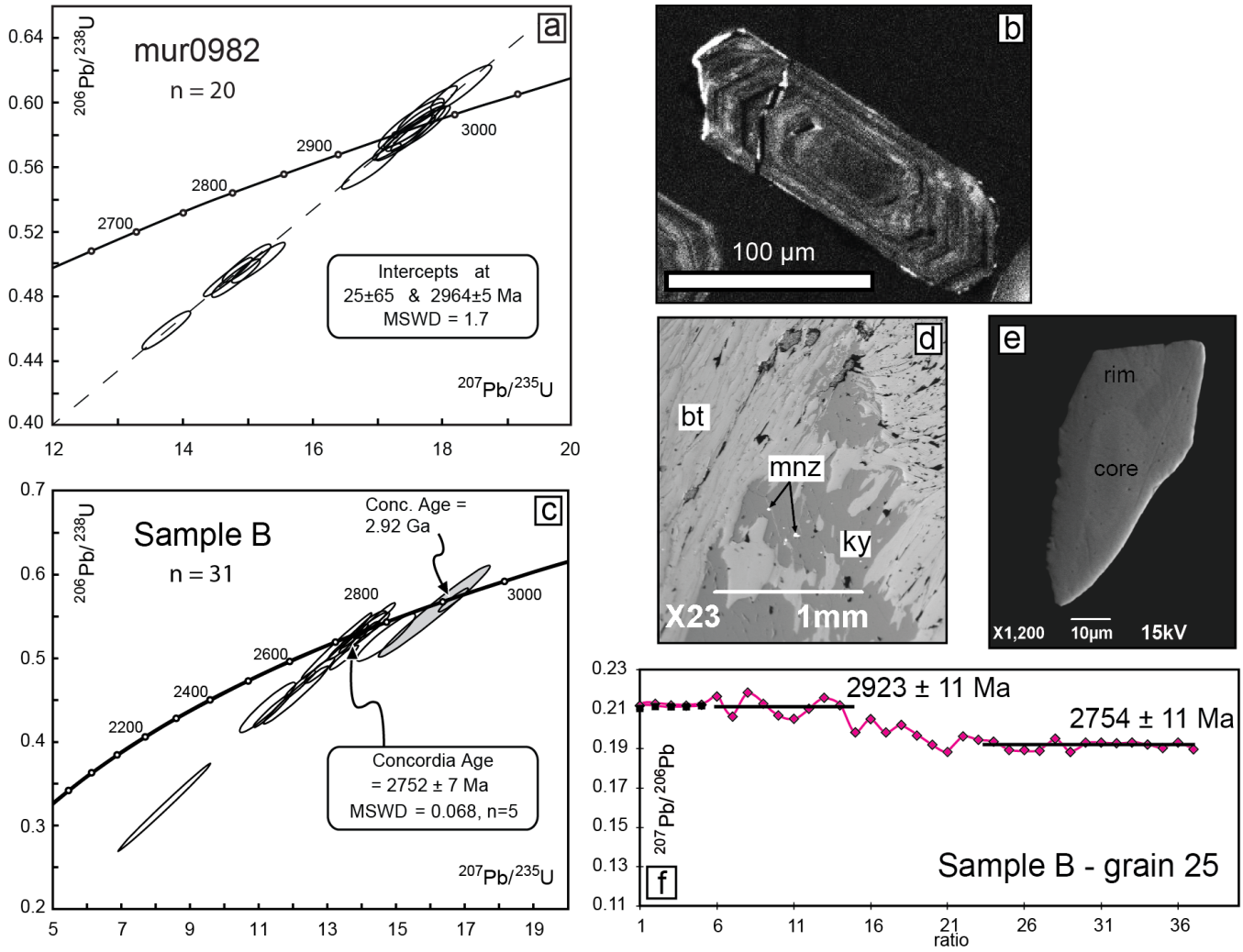

Figure 8:

Results of U-Pb LA-ICP-MS dating of zircon, monazite and xenotime from the La France Formation.

(a) Concordia diagram with results of U-Pb zircon dating of the granitoid sample mur0982 from the Letaba Shear Zone. An upper intercept age of 2966.7 ± 7.1 Ma was obtained. (b) Cathodoluminescence image of a zircon of sample mur0982. (c) Concordia diagram showing results of monazite and xenotime analysis of sample B of the La France Formation, with concordant ages at 2752 ± 7. (d) BSE image of monazite inclusions in a kyanite porphyroblast in sample B. (e) BSE image of a monazite inclusion in kyanite (sample B) revealing a complex zonation.
g) Time resolved $^{207}Pb/^{206}Pb$ signal obtained from a monazite inclusion in kyanite (mnz grain 25 - Table 3). Note the stepwise decrease of the $^{207}Pb/^{206}Pb$ signal, corresponding to an age decrease from 2923 ± 11 Ma to 2754 ± 11 Ma (2 sigma).

6. Discussion

6.1. Metamorphic conditions and geothermal gradients

The results of our P—T modelling reveal that the three investigated tectono-metamorphic units of the MGB underwent contrasted metamorphic evolutions. The volcano-sedimentary rocks of the Murchison Unit, that form the central part of the MGB, underwent metamorphism in the lower-greenschist to lower-amphibolite facies, at P—T conditions not exceeding 5-6.2 kbar and 530-570°C; peak metamorphic conditions being highly variable within this unit. In contrast, the La France Formation, on the southern edge of the MGB, underwent high grade amphibolite-facies metamorphism at conditions of 8 – 9 kbars, and temperatures of 600-650 °C, corresponding to higher-amphibolite facies conditions. They subsequently underwent near-isothermal decompression to under 6.2 kbar, with temperature between 600 and 660°C, followed by cooling to 570-610°C, at pressures in excess of 5 kbar. The Silwana Amphibolites sliver, on the north-western edge of the MGB, experienced a metamorphic overprint in the upper amphibolite facies under P—T conditions of 8.7 – 10 kbars, 630-670°C. Rocks of both units record a prograde pressure-temperature increase from about 4.5-5.5 kbars at 520-570°C towards the metamorphic peak. Furthermore, rocks of the La France Formation additionally provide evidence for a

complex retrograde P—T history, characterised by near-isothermal decompression from 9.0-6.8 to <6 kbar at 600-660 °C, followed by a nearly-isobaric cooling from 620-650 °C to 570-610°C at about 5.5 kbar, accompanied by a secondary H_2O-rich fluid enrichment.

Peak P—T conditions for the La France supracrustals and the Silwana Amphibolites require a burial to mid-crustal levels, at depths of 27 – 30 km and 29 – 33 km respectively. Bearing in mind that the pressures determined from peak assemblages are in fact minimal pressures due to possible re-equilibration of the thermodynamic systems along the high-grade portions of the retrograde path, these values represent minimal burial depths. Therefore, the La France Formation and the Silwana Amphibolites underwent metamorphism along fairly similar minimal apparent geothermal gradients of 19-24°C/km. Furthermore, a steep prograde P—T vector inferred for rocks from both formations, suggesting a fast burial. In contrast, much lower peak P—T conditions of 5-6.2 kbar and 550-570°C for sample M2 indicate that rocks of the Murchison Unit were buried at shallower depths of 16 – 20 km, along an apparent geotherm of 27-34 °C/km. The peak P—T conditions of metabasite sample M1 are even lower and require even higher apparent geotherms (40-80°C/km). The reasons for the different peak P—T conditions of the investigated rocks of Murchison Unit are not entirely clear. Apart from the fact that the peak pressures are not well constrained, in particular for sample M1, the enormous temperature differences could reflect either a metamorphic array (e.g. England & Thompson, 1984), whereby different slivers has reached different peak conditions at different times or, alternatively, a metamorphic gradient caused by magma intrusions within the MGB. A less likely option is that the enormous temperature difference represents an artefact of the used thermodynamic calculation method. If the latter holds true, the P—T results obtained from the metapelitic rocks are considered to be more appropriate than those from the metabasite, since thermodynamic activity models for metapelite phases are more robust and less sensitive to slight variations in Na, Ti and Fe^{3+} than those for metabasite phases, e.g. amphiboles (see Dale et al., 2005; Diener et al. 2007; Diener and Powell, 2010).

It is interesting to note that the maximum peak P—T conditions obtained for the Murchison Unit

(5.0-6.2 kbars at 530-570 °C) overlap with those inferred from the retrograde P—T evolution of the La France Formations (assemblage B3). Despite this coincidence, it remains unclear, whether the identical P—T conditions in both units were reached at the same time, meaning that prograde heating in the Murchison Unit ceased while rocks of the La France Formation underwent isothermal decompression. In any case, our results show that the three tectono-metamorphic units of the MGB were buried along different apparent geotherms, at different crustal depths, and experienced contrasted metamorphic evolutions before being juxtaposed.

6.2. Timing of the evolution of the MGB

A maximum age for metamorphism in the Murchison Unit is provided by the youngest (meta)volcanic rocks of the Rubbervale Formation of the MGB, dated at ca. 2.97 Ga (Brandl et al. 1996, Poujol et al. 1997, Poujol 2001). This age is identical within errors to the crystallisation age measured for the syn-deformation granitoid intrusive in the Letaba Shear Zone. It also is indistinguishable from the crystallisation ages of small granitoid bodies emplaced both along the Antimony Line (2970 ± 15 Ma Malati Pump granodiorite, Poujol et al. 1997), and to the south of the MGB (2969 ± 17 Ma Discovery granite, Poujol 2001). However, it is significantly older that the U-Pb ages of 2752 ± 7 Ma, and rarely of 2910-2920 Ma, obtained from the monazites and xenotimes of the La France micaschists. The older ages of ca. 2.92 Ga which were only obtained from monazite or xenotime inclusions in kyanite, are interpreted to reflect a minimum age for peak metamorphism in the La France Formation. It is worth noting that these ages are within error identical to the emplacement age of the post-deformation Maranda Granite which intruded the southern part of the MGB at 2901 ± 20 Ma (Poujol et al., 1996), pointing to a possible synchronism of magmatism and metamorphism. The younger monazite and xenotime age of 2752 ± 7 Ma may results from re-activation of the MGB related to thermal processes in the Rooiwater Complex of the MGB (minimal intrusion ages of 2740 ± 4 Ma: Poujol et al., 1996), or in the Pietersburg Greenstone Belt (intrusion of the Turfloop granite at ca. 2780 Ma; Henderson et al., 2000).

6.3. Deformation localisation along major tectonic breaks

The break in metamorphic conditions between the Silwana Amphibolites and the Murchison Unit greenschists requires a 9-23 km vertical displacement across the Letaba Shear Zone. Strain increases sharply from moderately deformed greenschists of the Murchison Unit to intensely sheared mylonites, to the amphibolitic gneiss of the Silwana Amphibolites, Furthermore, there is a marked change in deformation patterns across the shear zone, with a high-grade metamorphic flattening fabric, that formed during prograde metamorphism, in the Silwana Amphibolites, and low grade greenschist-facies mylonitic fabric, consistent with a sinistral strike-slip deformation, dominating in the Murchison Unit schists. The fabrics of the Letaba Shear Zone provide evidence for a general transpressive tectonic setting with a top-to-the-south transport. The structures observed in the Letaba Shear Zones suggest that the Silwana Amphibolites, formed at a low crustal level, were juxtaposed to the greenschist- to lower amphibolite-facies rocks of the Murchison Unit along a transpressive shear zone, that was activated due to sustained crustal shortening in a general N-S direction, and that accommodated a large vertical displacement. As crustal shortening and thickening were ongoing, the tectonic regime may have shifted from transpression with a strong reverse component and a top-to-the-south directed transport, to strike-slip shearing. Locally, conjugated SE-trending shear zones were activated together with the predominant NE-trending structures. This late stage of tectonic activity was accompanied by the intrusion of syntectonic granitoids in the Letaba Shear Zone at 2967 ± 7 Ma. These granitoids intruded prior to or during the sinistral slip under greenschist-facies conditions, as is well reflected by the S-C fabrics they display.

The La France Fault displays a number of similarities with the Letaba Shear Zone. It localises an important amount of deformation that accounts for a large vertical displacement of 7-20 kilometres. The fault zone also develops tectonic fabrics consistent with a general transpressive, sinistral regime and a

top-to-the-south transport direction. Deformation in the La France Formation shows patterns that are not seen elsewhere in the MGB. Deformation in the fault zone can be correlated with the D_3 deformation within the La France Formation, which is characterised by crenulations and small-wavelength open folds with shallow dipping axes. It post-dates the prograde P—T evolution of the La France Formation during the D_1 and D_2 deformation events. The structures of both shear zones illustrate a north-overriding-south relation.

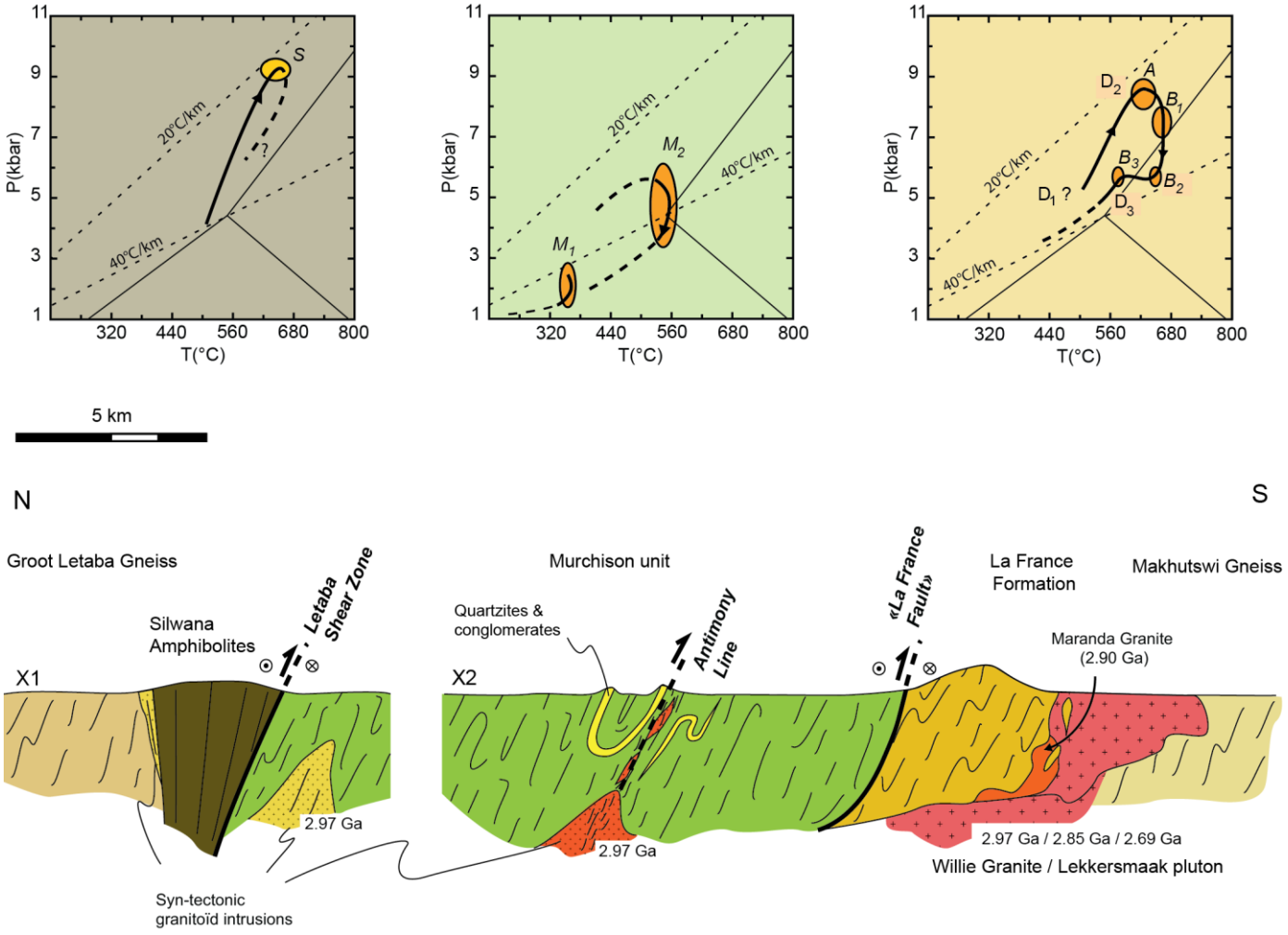

Figure 9:

Interpretative cross-section of the MGB. The MGB has an asymmetric structure, and structural units with distinct metamorphic P-T evolutions (see P—T diagrams) are juxtaposed along shear zones. The MGB is intruded by both syn-tectonic granitoids at 2.97 Ga and by late-stage granitoids as from 2.90 Ga. Profile lines labelled x1 and x2 are located on Fig. 2. Ellipses in the P – T diagrams indicate peak metamorphic and retrograde conditions obtained in this study.

Dark solid curves represent P—T path segments inferred from our results of P—T modelling, while dashed curves show presumed portions of the paths. Deformation events (D_1, D_2, D_3) and studied

assemblages (S, M_1, M_2, A, B_1, B_2, B_3) are shown along the P—T paths.

6.4. Model of the tectono-metamorphic evolution of the MGB

The structutral-metamorphic data obtained during this study, along with previous works (e.g., Vearncombe, 1988a, 1988b; Jaguin et al., 2012) indicate that the different units of the MGB underwent a similar style of penetrative, left-lateral deformation, as well as deformation localisation along the boundaries between units with contrasted metamorphic evolutions (Fig 9). These features could be accounted for by a sequential evolution model as follows: During the early stage of the evolution of the MGB, shortening was accommodated by crustal thickening due to thrusts and/or transpressive shear zone activation, whereby the different units underwent prograde metamorphism upon burial at lower to mid-crustal level, along moderate apparent geothermal gradients. At some point during the thickening-shortening process, the reverse component of the shear zones attenuated, as they evolved into a strike-slip regime. Shortening was no longer accommodated solely along the primary shear zones that localised deformation, but rather by a penetrative deformation distributed in the rocks of the MGB and surrounding terrains, and homogeneous, moderate crustal thickening, coincident with a metamorphic overprint along a high-T, low-P apparent geothermal gradient. Our results allow to suggest that the tectonic juxtaposition of the Murchison Unit and La France Formation took place following crustal thickening, after peak metamorphism and partial exhumation of the La France Formation, at which point the latter and a portion of the Murchison Unit underwent a similar metamorphic evolution. The greenschist-facies metamorphism of the Murchison Unit may have been locally overprinted by a slightly higher-grade metamorphism as a consequence of tectonic accretion. Similarly, the final juxtaposition of the Silwana Amphibolites to the rest of the belt occurred after peak metamorphism and exhumation, along a late-stage strike-slip shear zone.

6.5. Implications for Archaean tectonic regimes

It is generally assumed that a higher average geothermal gradient prevailed in Archaean lithospheres relative to modern ones, thus maintaining weak lithospheres unable to withstand thickening (e.g. Rey and Houseman, 2006). Furthermore, a hot, more buoyant sub-continental lithospheric mantle in the Archaean (Griffin et al., 1998) would have inhibited lithosphere thickening by stacking in Archaean collisional belts, as it would have enhanced gravitational potential energy build-up as relief formed. Therefore, in an Archaean context, it is expected that convergence be accommodated by moderate thickening in its early stage, but quickly volume forces would become dominant on boundary stresses as gravitational potential energy builds up with increased thickening. Further thickening would be limited, and shortening would be accommodated by lateral escape of material, leading to a steady state where lithospheric thickness remains constant as long as convergence goes on (Rey and Houseman, 2006). This shift between the dominance of boundary stress to volume forces would correspond to the transition from a tectonic regime dominated by oblique thrusting to one marked by strike-slip shearing. It has been recognised in the sequential evolution of a number of Archaean and Palaeoproterozoic orogens (e.g. Kusky and Polat, 1999, in the Superior province, Feybesse et al., 2006 in the Birimian of the West African Craton). On Archaean lithospheres, the threshold controlling this transition would be reached much earlier than in Phanerozoic orogens, thus aborting pronounced thickening.

The cold apparent geothermal gradients inferred for the La France Formation and Silwana Amphibolites of the Murchison Greenstone Belt are comparable to those encountered in collisional belts in Proterozoic and Phanerozoic orogens (Brown, 2009). Burial along low geothermal gradients to about 30 km implies that the lithosphere strength was sufficient to sustain substantial thickening and loading, at least for a period of time. Weakening of the crust could therefore not have occurred before burial of supracrustal sequences at mid-crustal depths. In fact, the P –T paths followed by the La France Formation and the Silwana Amphibolites (Fig 9) inferred from our result are at odds with P—T paths expected from metamorphic terrains in hot orogens (Chardon et al, 2009; Gapais et al, 2009). Indeed, P—T paths

followed by particles in hot orogens are reported to show cooling during decompression, a sign that exhumation is slow enough to enable thermal reequilibration (e.g., P-T paths from the Limpopo Belt: Zeh et al., 2004; Millonig et al., 2010). In contrast, the Silwana Amphibolites and La France Formation underwent a relatively fast burial, as is indicated by steep prograde P-T vectors, followed, for the latter, by a near-isothermal decompression. These features suggest that isotherms were not parallel to the surface at the time of metamorphism, and consequently exhumation must have been driven by tectonic processes rather than by homogeneous erosion. An intermediate model between typical Archaean and Phanerozoic orogens, where crustal shortening is accommodated by moderate crustal thickening, by deformation localisation along transpressive shear zones, as well as by strike-slip shearing and strain distribution at a regional scale, would better account for the tectono-metamorphic features of the MGB (e.g. Cagnard et al., 2011).

The results of this study echo the metamorphic conditions reported in the south of the older, 3.5 – 3.2 Ga, Barberton Greenstone Belt (Dziggel et al., 2002 ; Diener et al., 2005 ; Moyen et al., 2006). The tectono-metamorphic evolution of the BGB shows similar thermal and mechanical properties of the lithosphere of the Kaapvaal Craton before the formation of the MGB. It therefore seems likely that the Kaapvaal Craton was a rather cold craton compared to other Archaean provinces, thus illustrating certain variability in geodynamic processes within the Archaean.

7. Conclusion

The Murchison Greenstone Belt is a narrow volcano-sedimentary belt comprising various terrains that have been tectonically juxtaposed. The geological units that represent most of the belt underwent lower-greenschist to lower-amphibolite facies metamorphism along a relatively hot, ~30°C/km apparent geothermal gradient. Two small slivers, at the north-eastern and southern edges of the MGB respectively, were metamorphosed in the higher amphibolite facies. They underwent burial at more than 30 km deep

along a relatively cold, ~20°C/km geotherm. The contact zones between the low-grade and high-grade formations are narrow and sharp. They represent high-strain shear zones that account for major breaks in metamorphic conditions across the belt. While deformation due to shortening is distributed at a regional scale, we show that shortening was also accommodated by localisation of deformation along transpressive, sinistral tectonic contacts accompanied by a top-to-the-south directed transport. This mode of shortening accounted for the final juxtaposition of terrains that were metamorphosed at different crustal levels in the MGB.

The evolution of orogenic belts during shortening, from a tectonic regime dominated by thrusting, thickening, and deformation localisation coincident with prograde metamorphism, to one dominated by strike-slip shearing, lateral flow and deformation distribution accompanied by retrograde metamorphic overprints, is not specific of or restricted to any time period in the geological record. As shown by our results and by studies of the Barberton Greenstone Belt, moderate thickening, high-P, moderate- to low-T metamorphism and high metamorphic gradients do occur in the Archaean. However, secular changes in the heat budget of the Earth must have affected the relative importance of the different modes of shortening, and probably account for the clearly contrasting tectonic features between the Archaean and Proterozoic eras. In any case, drawing geodynamic models illustrating the differential behaviour of Archaean and Proterozoic orogens should not be done without a consideration for the possible variations of the parameters determining the rheological profiles and, as a consequence, the behaviour of lithospheres at a given age.

Appendix

A.1. XRF and microprobe analysis

Whole rock chemistry analyses were obtained using an ACME at University of Stellenbosch, South Africa. Complementary analyses were obtained by XRF at the CRPG in Nancy and the at the Ecole des

Mines in Saint-Etienne. Mineral chemical analyses were performed on a LEO 140VP scanning electron microscope coupled to a Link ISIS energy dispersive spectrometry system at the University of Stellenbosch. The microscope was operated at 20 kV with a beam current of 120A and a probe current of 1.5 nA. Acquisition time was set at 50 s and spectra were processed by ZAF corrections and quantified using natural mineral standards. Details of the analytical procedure are provided in Diener et al. (2005). Complementary analyses were carried out at the Electron Microprobe Laboratory at Université Blaise Pascal in Clermont-Ferrand, France, using a Cameca SX 100 electron microprobe analyser. Operating conditions were 20 kV, 20 nA, 5–10 μm beam size and counting time of 10s per element. Natural silicates were used as standards. The analyses carried out in the different laboratories were identical within errors.

A.2. Pseudosection calculation

Pseudosections of rocks from the different terrains of the MGB were constructed using the Peple_X software (Connolly and Kerrick, 1987; Connolly, 2005; 2009) in the Na_2O–CaO–K_2O–FeO–(Fe_2O_3–)MgO–MnO–Al_2O_3–TiO_2–SiO_2–H_2O system, and using the thermodynamic database hp04 of Holland and Powell (1998, revised 2004). The solution models used for the pseudosections are as follows : Bio(TCC) for biotite (Tajcmanova et al., 2009), Chl(HP) for chlorite (Holland et al., 1998), St(HP) for staurolite (Powell et al., 1998), Ctd(HP) for chloritoïd (Holland and Powell), Amph(DPW) for amphibole (Dale et al., 2005), Gt(WPH) for garnet (White et al., 2000), Ilm(WPH) for ilmenite (White et al., 2000), hCrd for cordierite, Mica(CHA1) for titanium bearing white mica (Coggon and Holland, 2002, Auzanneau et al., 2010), Pheng(HP) for phengite (Holland and Powell 1998), melt(HP) (Holland and Powell, 2001), Pl(h) for plagioclase feldspar (Newton et al. 1981), Kf for potassic feldspar (Waldbaum and Thompson 1968), Opx(HP) for orthopyroxene (Holland and Powell, 1996), Cpx (HP) for clinopyroxene (Holland and Powell, 1996). Pseudosections were first built by using the bulk rock composition obtained by XRF analysis of each sample. However, this method failed to model accurately the observed assemblages and mineral compositions for samples bearing large, centimetric minerals. For

such samples, the bulk rock composition was calculated from the mineral modes and average mineral compositions (e.g. samples A, B and S, Table 4). Modal proportions were estimated by image analysis, and average mineral compositions were obtained by averaging a large number of microprobe analyses acquired on minerals of a single thin section. In order to show the effect of garnet fractionation on the P—T pseudosection topology (e.g., sample A), we obtained the total bulk compositions by XRF, as well as the effective bulk composition after porphyroblast garnet growth, by subtracting the core composition of the zoned garnet grains (ca. 10 vol.%) from the total bulk composition, using a method similar to the procedure described by Marmo et al. (2002) and Zeh et al. (2006).

Whole rock XRF (wt%) - all Fe as Fe^{2+}						Recalculated (wt%)				
	A	B	M1	M2	S		A with Gt cores	A without Gt cores	B	S
SiO_2	75.62	56.51	62.55	92.99	55.68	SiO_2	61.67	64.24	47.00	52.41
Al_2O_3	11.76	17.39	6.96	2.84	12.09	Al_2O_3	15.30	14.73	23.75	12.61
FeO	6.68	8.08	7.13	1.77	16.21	FeO	14.97	12.87	9.54	22.01
MnO	0.04	0.07	0.14	0.10	0.18	MnO	0.51	0.19	0.00	0.52
MgO	1.52	8.45	12.32	0.54	2.77	MgO	1.73	1.75	8.44	2.64
CaO	< D.L.	0.52	5.58	0.07	7.19	CaO	0.46	0.27	0.30	6.08
Na_2O	0.17	0.61	1.27	0.00	2.89	Na_2O	0.12	0.13	0.50	1.16
K_2O	2.64	4.87	0.02	0.58	0.24	K_2O	1.92	2.12	6.41	0.29
TiO_2	0.20	0.58	0.30	0.10	2.04	TiO_2	0.19	0.21	0.63	0.84
P_2O_5	0.17	b.d.l.	0.02	0.00	0.81	H_2O	1.50	1.50	sat.	sat.
LOI	2.35	2.99	3.40	1.06	0.89	Fe_2O_3	0.00	0.00	0.00	0.00
Total	101.15	100.07	99.69	100.05	100.99	Total	98.37	98.01	96.57	98.56

Table 4:

Whole rock compositions of the studied samples. The pseudosections of samples from the Murchison Unit (M1 and M2) were built using the whole rock compositions obtained by XRF analysis. Whole rock compositions were recalculated for the other samples to take into account the effect of large porphyroblasts on the composition of an equilibration volume (samples A, B and S) or to correct the effect of accessory phases (sample S, see appendix A2).

Fe_2O_3 of the bulk rock was estimated by calculating the Fe^{3+} content of normalised structural formulae of analysed minerals (Droop, 1987) and from mineral modes. By applying this procedure we obtained Fe_2O_3 contents of less than 0.05 wt% for all samples. T – X pseudosections were constructed to test the

implications of approximating all Fe as Fe^{2+}. In all cases, the consequences in terms of phase compositions and proportions were found to be negligible. Thus, Fe_2O_3 as a system component was ignored during this study, since it is little influential. Other corrections included correcting whole rock Ca content for apatite and calcite in the studied sample, using calcite modal proportions and bulk P_2O_5 composition. As a general rule, oxydes with a bulk rock content <0.05 wt% were ignored for pseudosection calculations.

The prograde history of fluid-bearing mineral assemblages involves the progressive dehydration and fluid loss with rising temperature. The water content of a rock decreases along the prograde path and reaches a minimum at peak metamorphic conditions. Unless a secondary water enrichment occurs (such as documented in sample B), the water content along the retrograde path is assumed to be close to the water content at peak T conditions. As the retrograde assemblages of the investigated samples require a post-peak metamorphism water influx, the P—T pseudosections for all samples were constructed under the assumption that water was in excess throughout the entire metamorphic history.

A.3. LA-ICP-MS U-Th-Pb dating

A classic mineral separation procedure has been applied to concentrate zircon grains using the facilities available at Géosciences Rennes. Rocks were crushed and only the powder fraction with a diameter < 250 µm was kept. Heavy minerals were successively concentrated by Wilfley table and heavy liquids. Magnetic minerals were then removed with an isodynamic Frantz separator. Zircon grains were handpicked under a binocular microscope and embedded in epoxy mounts. The grains were then hand-grounded and polished on a lap wheel with a 6 µm and 1 µm diamond suspension successively. Zircons were imaged by cathodoluminescence (CL) using a Reliotron CL system equipped with a digital color camera available in Géosciences Rennes.

U-Th-Pb geochronology of zircon from the sample mur0982 was conducted by in-situ laser ablation inductively coupled plasma mass spectrometry (LA-ICPMS) at the Laboratoire Magmas et

Volcans in Clermont-Ferrand, France, using a Resonetics M-50E 193 nm ArF excimer NewWave UP213 laser system, with a laser spot diameter of 26 µm and repetition rates of 3 Hz. Data were corrected for U–Pb fractionation and for the mass bias by standard bracketing with repeated measurements of the GJ-1 zircon (Jackson et al., 2004). Data reduction was carried out with the GLITTER® software package developed by the Macquarie Research Ltd. (Jackson et al., 2004). Further information on the instrumentation and the analytical technique is detailed in Hurai et al. (2010).

U-Pb dating of monazite and xenotime was carried out on polished thin sections at Goethe University Frankfurt, Germany. Prior to the U-Pb dating, the internal structures of the grains were investigated by back-scattered electron (BSE) imaging using a ThermoScientific Element 2 sector field ICP-MS coupled to a Resolution M-50 (Resonetics) 193 nm ArF excimer laser (ComPexPro 102F, Coherent) system. Data were acquired in time resolved – peak jumping – pulse counting / analogue mode over 356 mass scans, with a 20 second background measurement followed by 21 second sample ablation. Laser spot-size for monazite and xenotime are 15 µm, and 23 µm for the standard zircons GJ1. Ablations were performed in a 0.6 L min^{-1} He stream, which was mixed directly after the ablation cell with 0.07 L min^{-1} N_2 and 0.68 L min^{-1} Ar prior to introduction into the Ar plasma of the SF-ICP-MS. All gases had a purity of >99.999% and no homogeniser was used while mixing the gases to prevent smoothing of the signal. Signal was tuned for maximum sensitivity for Pb and U while keeping oxide production, monitored as $^{254}UO/^{238}U$, below 0.5%. The sensitivity achieved was in the range of 9000-14000 cps/µg g^{-1} for ^{238}U with a 23 µm spot size, at 5.5 Hz and 5-6 J cm^{-2} laser energy. The two-volume ablation cell (Laurin Technic, Australia) of the M50 enables detection and sequential sampling of heterogeneous grains (e.g., growth zones) during time resolved data acquisition, due to its quick response time of <1s (time until maximum signal strength was achieved) and wash-out (< 99.9% of previous signal) time of about 2s. With a depth penetration of ~0.7 $µms^{-1}$ and a 0.46s integration time (4 mass scans = 0.46 s = 1 integration) any significant variation of the Pb/Pb and U/Pb in the µm scale is detectable. Raw data were corrected offline for background signal, common Pb, laser induced elemental fractionation, instrumental

mass discrimination, and time-dependent elemental fractionation of Pb/U using an in-house MS Excel© spreadsheet program (Gerdes and Zeh, 2006; 2009). A common-Pb correction based on the interference- and background-corrected ^{204}Pb signal and a model Pb composition (Stacey & Kramers 1975) was carried out. The ^{204}Pb content for each ratio was estimated by subtracting the average mass 204 signal, obtained during the 20 second baseline acquisition, which mostly results from ^{204}Hg in the carrier gas (c. 180-420 cps), from the mass 204 signal of the respective ratio. For the analyzed sample the calculated common ^{206}Pb contents was mostly <1% of the total ^{206}Pb (see Table 3). For more details about data processing see (Gerdes and Zeh, 2006; 2009). The data were plotted using the software ISOPLOT (Ludwig 2001).

Acknowledgements

The authors thank Michael Brown for his detailed review of the manuscript which contributed to improve significantly the quality of the work. Timothy Kusky and an anonymous reviewer are also thanked for their constructive comments. The participation of Arnaud Villaros through discussions and advice was greatly appreciated. Preliminary results of this study were presented at the 5th International Archaean Symposium in Perth in 2010 thanks to a travel grant provided by Geoconferences (WA) Inc. Armin Zeh also thanks the Deutsche Forschungsgemeinschaft, grant ZE 424/11-1, for financial support.

References

Altermann, W. and Nelson, D.R.., 1998. Sedimentation rates, basin analysis and regional correlations of three Neoarchaean and Palaeoproterozoic sub-basins of the Kaapvaal Craton, Northern Cape Province, South Africa. J. Afr. Earth Sci., **13**, 415-435.

Anhaeusser, C.R., 2006. A reevaluation of Archean intracratonic terrane boundaries on the Kaapvaal Craton, South Africa: Collisional suture zones? GSA Special Papers 2006, 405 193-210

Auzanneau, E., Schmidt, M.W., Vielzeuf, D., Connolly, J.A.D., 2010. Titanium in phengite: a geobarometer for high temperature eclogites. Contrib. Mineral. Petrol. 159, 1-24.

Berthé, D., Choukroune, P., Jegouzo, P., 1979. Orthogneiss, mylonite and non-coaxial deformation of granites : the example of the South Armorican shear zone. J. Struct. Geol. 1, 31-43.

Binns, R.A., Gunthrope, R.J. and Groves, D.I., 1976. Metamorphic patterns and development of greenstone belts in the eastern Yilgarn Block, Western Australia. In: Windley, B.F. (ed.). The Early History of the Earth. Wiley, New York, N.Y., 303–316.

Bouhallier, H., Choukroune, P. and Ballevre, M., 1993. Diapirism, bulk homogenous shortening and transcurrent shearing in the Archaean Dharwar craton: the Holenarsipur area. Precambrian Res., 63, 43–58.

Bouhallier, H., Chardon, D., Choukroune, P., 1995. Strain patterns in Archaean dome-and-basin structures: the Dharwar craton (Karnataka, South India). Earth Planet. Sci. Lett. 135, 57–75.

Brandl, G., Kröner, A., 1993. Preliminary results of single zircon studies from various Archaean rocks of the Northeastern Transvaal. In: Ext. Abstr. 16th International Colloquium of African Geology, Mbabane, Swaziland, 54–56.

Brandl, G., Jaeckel, P., Kröner, A., 1996. Single zircon age for the felsic Rubbervale Formation, Murchison greenstone belt, South Africa. S. Afr. J. Geol. 99, 3, 229–234.

Brandl, G., Cloete, M., Anhaeusser, C.R., 2006. Archaean Greenstone Belts, In: Johnson, M.R.,

Anhaeusser, C.R., Thomas, R.J., The Geology of South Africa, 2006.

Brown, M., 2007. Metamorphic conditions in orogenic belts: a record of secular change. Int. Geol. Rev. 49:193–234

Brown, M., 2009. Metamorphic patterns in orogenic systems and the geological record. In: Cawood PA, Kroner A (eds) Earth accretionary systems in space and time, vol 318. Geol. Soc. Lond. Spec. Publ., 37–74

Brown, M., 2010. Paired metamorphic belts revisited. Gondwana Research 18, 46–59.

Burger, A.J., Coertze, F.J., 1973. Radiometric age measurements on rocks from southern Africa to the end of 1971. Bull. Geol. Surv. S. Afr. 58, 46–46.

Caby, R., Delor, C., Agoh, O., 2000. Lithologie, structure et métamorphisme des formations birimiennes dans la région d'Odienné (Côte d'Ivoire): rôle majeur du diapirisme des plutons et des décrochements en bordure du craton de Man. J. Afr. Earth Sci. 30, 351–374.

Cagnard, F., Barbey, P., Gapais, D., 2011. Transition between “Archaean-type” and “modern-type” tectonics : Insights from the Finnish Lapland Granulite Belt. Precambrian Res. 187, 127–142.

Cawood, P., Kröner, A., Collins, W.J. et al., 2009. Accretionary orogens through Earth histoiry. Geol. Soc. Lond. Spec. Publ., 318, 1-36.

Chardon, D., Choukroune, P., Jayananda, M., 1996. Strain patterns, décollement and incipient sagducted greenstone terrains in the Archaean Dharwar craton (South India). J. Struct. Geol. 18, 991–1004.

Chardon, D., Choukroune, P., Jayananda, M., 1998. Sinking of the Dharwar basin (South India): implications for Archaean tectonics. Precambrian Res. 91, 15–39.

Chardon, D., Andronicos, C.L., Hollister, L.S., 1999. Large-scale transpressive shear zone patterns and displacements within magmatic arcs: the Coast Plutonic Complex, British Columbia. Tectonics 18, 278–292.

Chardon, D., Jayananda, M., Chetty, T.R.K., Peucat, J.-J., 2008. Precambrian continental strain and shear zone patterns: South Indian case. J. Geophys. Res. 113, B08402, doi:10.1029/2007JB005299.

Chardon, D., Gapais, D., Cagnard, F., 2009. Flow of ultra-hot orogens: a view from Precambrian, clues for the Phanerozoic. Tectonophysics 477 (3–4), 105–118.

Chopin, C., 1984. Coesite and pure pyrope in high-grade blueschists of the western Alps: a first record and some consequences. Contrib. Mineral. Petrol. 86, 107–118.

Choukroune, P., Bouhallier, H., Arndt, N.T., 1995. Soft lithosphere during periods of Archean crustal growth or crustal reworking. In: Coward, M.P., Ries, A.C. (Eds.), Early Precambrian Processes. Geol. Soc. Spec. Publ., 95, 67–86.

Choukroune, P., Ludden, J.N., Chardon, D., Calvert, A.J., Bouhallier, H., 1997. Archaean crustal growth and tectonic processes: a comparison of the Superior Province, Canada and the Dharwar craton, India. In: Burg, J.-P., Ford, M. (Eds.), Orogeny through Time. Geol. Soc. Spec. Publ., 121, 63–98.

Coggon, R., Holland, T.J.B., 2002. Mixing properties of phengitic micas and revised garnet-phengite thermobarometers. J. Metamorph. Geol. **20**, 683-96.

Collins, W.J., Vernon, R.H., 1991. Orogeny associated with anticlockwise P–T-t paths: evidence from low-P, high-T metamorphic terranes in the Arunta inlier, central Australia. Geology 19, 835–838.

Compston, W., Kröner, A., 1988. Multiple zircon growth within early Archean tonalitic gneiss from the Ancient Gneiss Complex, Swaziland. Earth Planet. Sci. Lett. 87, 13–28.

Connolly, J. A. D., 2005. Computation of phase equilibria by linear programming : A tool for geodynamic modeling and its application to subduction zone decarbonation. Earth Planet. Sci. Lett. 236, 524-541.

Connolly, J. A. D., 2009. The geodynamic equation of state : what and how. Geochemistry, Geophysics, Geosystems 10**.**

Connolly, J. A. D. and Kerrick, D.M., 1987. An algorithm and computer program for calculating composition phase diagrams. CALPHAD 11:1-

Condie, K. C. and Kröner, A., 2008. When did plate tectonics begin? Evidence from the geologic record in Condie, K. C. and Pease, V. eds. When Did Plate Tectonics Begin on Planet Earth? Geological Society of America Special Paper 440, 281-294, doi: 10.1130/2008.2440(14).

Dale, J., Powell, R., White, R.W., Elmer, F.L., Holland, T.J.B., 2005. A thermodynamic model for Ca-Na clinoamphiboles in Na2O-CaO-FeO-MgO-Al2O3-SiO2-H2O-O for petrological calculations. J. Metamorph. Geol. 23, 771-91.

Diener, J.F.A, Stevens, G., Kisters, A.F.M, Poujol, M., 2005. Metamorphism and exhumation of the basal parts of the Barberton greenstone belt, South Africa: Constraining the rates of Mesoarchaean tectonism. Precambrian Res.143, 87–112.

Diener, J.F.A., Powell, R., White, R.W., & Holland, T.J.B., 2007. A new thermodynamic model for clino- and orthoamphiboles in the system Na2O-CaO-FeO-MgO-Al2O3-SiO2-H2O-O. J. Metamorph. Geol., 25, 631-656.

Diener, J.F.A., Powell, R., 2010. Influence of ferric iron on the stability of mineral assemblages. J. Metamorph. Geol., 28, 599–613.

De Wit, M., 2004. Archean greenstone belts do contain fragments of ophiolites. In Condie, K. C., Kusky, T. M. (Editors), Precambrian Ophiolites and Related Rocks, Developments in Precambrian Geology v. 13, Elsevier Publishers.

Droop, G.T.R., 1987. A general equation for estimating Fe^{3+} concentrations in ferromagnesian silicates and oxides from microprobe analyses, using stoichiometric criteria. Mineralogical Magazine, 51 (3), 361, 431-435.

Du Plessis, C. P., 1990. Tectonism along the Thabazimby-Murchison lineament. Ph.D. Thesis (unpubl.), Univ Witwatersrand, Johannesburg, 243 pp.

Dziggel, A., Stevens, G., Poujol, M., Anhaeusser, C.R., Armstrong, R.A., 2002. Metamorphism of the granite–greenstone terrane south of the Barberton greenstone belt, South Africa: an insight into the tectono-thermal evolution of the ‘lower’ portions of the Onverwacht Group.

Precambrian Res. 114, 221–247.

England, P. C. and Thompson, A. B., 1984. Pressure – temperature – time paths of regional metamorphism, Part I; heat transfer during the evolution of regions of thickened continental crust. J. Petrol., 25, 894-928.

Ernst, W.G., 1973. Blueschist metamorphism and*P–T* regimes in active subduction zones. Tectonophysics 17, 255–272.

Ernst, W.G., 1975. Systematics of large-scale tectonics and age progressions in Alpine and circum-Pacific blueschist belts. Tectonophysics 26, 229–246.

Ernst, W.G., 1988. Tectonic history of subduction zones inferred from retrograde blueschist P—T paths. Geology 16, 1081–1084.

Evans, T. P., 2004. A method for calculating effective bulk composition modification due to crystal fractionation in garnet bearing schist: implications for isopleth thermobarometry. J. Metamorph. Geol. 22, 547–557.

Feybesse, J.-L., Billa, M., Guerrit, C., Duguey, E., Lescuyer, J.-L., Milesi, J.P., Bouchot, V., 2006. The paleoproterozoic Ghanaian province : Geodynamic model and ore controls, including regional stress modeling. Precambrian Res. 149, 149-196.

Florence, F. P. and Spear, F. S., 1991. Effects of diffusional modification of garnet growth zoning on P-T path calculations. Contrib. Mineral. Petrol., 107, 487-500.

Gapais, D., Cagnard, F., Gueydan, F., Barbey, P., Ballèvre, M., 2009. Mountain building and exhumation processes through time: inferences from nature and models. Terra Nova 21, 188–194.

Gerdes, A. and Zeh, A., 2006. Combined U-Pb and Hf isotope LA-(MC)ICP-MS analyses of detrital zircons: Comparison with SHRIMP and new constraints for the provenance and age of an Armorican metasediment in Central Germany. Earth and Pl. Sci. Letters 249, 47-61.

Gerdes, A. and Zeh, A., 2009. Zircon formation versus zircon alteration: new insights from combined U-Pb and Lu-Hf in-situ LA-ICP-MS analyses, and consequences for the interpretation of Archaean zircon from the Central Zone of the Limpopo Belt. Chem. Geol. 261, 230-243.

Good, N. and M.J. De Wit, 1997. The Thabazimbi-Murchison Lineament of the Kaapvaal craton, South Africa : 2700 Ma of episodic deformation. Journal of the Geological Society 154, 1, 93-97.

Grambling, J.A., 1986. Crustal thickening during Proterozoic metamorphism and deformation in New Mexico. Geology 14, 149–152.

Griffin, W.L., O'Reilly, S.Y., Ryan, C.G., Gaul, O., Ionov, D., 1998. Secular variation in the composition of the subcontinental lithospheric mantle. In: Braun, J. et al. (eds). Structure and Evolution of the Australian Continent, Geodynamics Series, 26, American Geophysical Union, 1–25.

Henderson, D.R., Long, L.E. and Barton, J.M., 2000. Isotopic ages and chemical and isotopic compositions of the Archaean Turfloop Batholith, Pietersburg granite-greenstone terrane, Kaapvaal Craton, South Africa. S. Afr. J. Geol., 103(1): 38-46.

Hurai, V., Paquette, J.-L., Huraiová, M., Konečný, P., 2010. U-Th-Pb geochronology of zircon and monazite from syenite and pincinite xenoliths in Pliocene alkali basalts of the intra-Carpathian back-arc basin. J. Volcanol. Geotherm. Res., 198, 275-287.

Holland, T., Powell, R., 1996. Thermodynamics of order-disorder in minerals. 2. Symmetric formalism applied to solid solutions. Am. Min. **81**, 1425-37.

Holland, T.J.B. and Powell, R., 1998. An internally consistent thermodynamic data set for phases of petrological interest. J. Metamorph. Geol. **16**, 309-43

Holland, T., Baker, J., Powell, R. 1998. Mixing properties and activity-composition relationships of chlorites in the system MgO-FeO-Al_2O_3-SiO_2-H_2O. European Journal of Mineralogy **10**, 395 406.

Holland, T., Powell, R., 2001. Calculation of phase relations involving haplogranitic melts using an internally consistent thermodynamic dataset. J. Petrol. **42**, 673-83.

Jaguin, J., Gapais, D., Poujol, M. , Boulvais, P. et Moyen, J.F. (in press). The Murchison Greenstone Belt (South Africa) : a general tectonic framework. S.Afr.J.Geol., 115, 1, 65-76.

Jackson, S.E., Pearson, N.J., Griffin, W.L., Belousova, E.A., 2004. The application of laser ablation-inductively coupled plasma-mass spectrometry to in situ U–Pb zircon geochronology. Chem. Geol., 211, 47–69.

Kamo, S.L., Davis, D.W., 1994. Reassessment of Archaean crustal development in the Barberton Moutain Land, South Africa, based on U–Pb dating. Tectonics 13 (1), 167–192.

Kisters, A.F.M., Stevens, G., Dziggel, A., Armstrong, R.A., 2003. Extensional detachment faulting and core-complex formation in the southern Barberton granite-greenstone terrain, South Africa: evidence for a 3.2 Ga orogenic collapse. Precambrian Res. 127, 355–378.

Komiya, T., Maruyama, S., Masuda, T., Nobda, S., Hayashi, M. & Okamoto, K. 1999. Plate tectonics at 3.8–3.7 Ga: Field evidence from the Isua Accretionary Complex, southern West Greenland. Journal of Geology, 107, 515–554.

Komiya, T., Hayashi, M., Maruyama, S. and Yurimoto, H., 2002. Intermediate-P/T type Archaean metamorphism of the Isua supracrustal belt: Implications for secular change of geothermal gradients at subduction zones and for Archaean plate tectonics. American Journal of Science, 302, 806–826.

Kröner, A., Byerly, G.R., Lowe, D.R., 1991. Chronology of early Archean granite–greenstone evolution in the Barberton Moutain Land, South Africa, based on precise dating by single grain zircon evaporation. Earth Planet. Sci. Lett. 103, 41–54.

Kröner, A., Hegner, E., Byerly, G.R., Lowe, D.R., 1992. Possible terrane identification in the early Archaean Barberton greenstone belt, South Africa, using single zircon geochronology. EOS Trans. AGU, Fall Meeting Suppl. 73 (43), 616.

Kröner, A., Tegtmeyer, A., 1994. Gneiss–greenstone relationships in the Ancient Gneiss Complex of southwestern Swaziland, southern Africa, and implications for early crustal evolution. Precambrian Res. 67, 109–139.

Kröner, A., Hegner, E., Wendt, J.I., Byerly, G.R., 1996. The oldest part of the Barberton granitoid–

greenstone terrain, South Africa: evidence for crust formation at 3.5 and 3.7 Ga. Precambrian Res. 78, 105–124.

Kröner, A., Jaeckel, P., Brandl, G., 2000. Single zircon ages for felsic to intermediate rocks from the Pietersburg and Giyani greenstone belts and bordering granitoid orthogneisses, northern Kaapvaal Craton, South Africa. J. Afr. Earth Sci. 30 (4), 773– 793.

Kusky, T. M., 1991. Structural development of an Archean orogen, western Point Lake, Northwest Territories. Tectonics, 10, 4, p. 820-841.

Kusky, T.M., Vearncombe, J.R., 1997. Structural aspects. In: de Wit, M., Ashwal, L.D. (Eds.), Greenstone Belts. Oxford Monogr. Geol. Geophys. 35, 91–124.

Kusky, T. M. and Polat, A. 1999. Growth of granite–greenstone terranes at convergent margins, and stabilization of Archean cratons. Tectonophysics 305, 43–73

Kusky, T.M., Li, Jianghai, and Tucker, R.T., 2001. The Archean Dongwanzi ophiolite complex, North China Craton: 2.505 Billion Year Old Oceanic Crust and Mantle, Science, 292, 1142-1145.

Ludwig, K.R., 1998. On the Treatment of Concordant Uranium-Lead Ages. GeCA, 62, 4, 665-676.

Ludwig, K.R., 2001. Isoplot/Ex, rev. 2.49: a geochronological toolkit for Microsoft Excel. Berkeley Geochronology Center, Spec. Publ. 1a, 55 p.

Marmo, B.A., Clarke, G.L., Powell, R., 2002. Fractionation of bulk rock composition due to porphyroblast growth : effects on eclogite facies mineral equilibria, Pam Peninsula, New

Caledonia. J. Metamorph. Geol., 20, 151-165.

Millonig, L., Zeh, A., Gerdes, A. & Klemd, R. (2008). Neoarchaean high-grade metamorphism in the Central Zone of the Limpopo Belt (South Africa): Combined petrological and geochronological evidence from the Bulai pluton. Lithos, **103**, 333-351.

Millonig, L., Zeh, A., Gerdes, A., Klemd, R., Barton, J.M., 2010. Decompressional Heating of the Mahalapye Complex (Limpopo Belt, Botswana): a Response to Palaeoproterozoic Magmatic Underplating ? J. Petrol. 51, 3, 703-729.

Mints, M. V., Belousova, E. A., Konilov, A. N., Natapov, L. N., Shchipansky, A. A., Griffin, W. L., O'Reilly, S. Y., Dokukina, K. A., Kaulina, T. V., 2010. Mesoarchean subduction processes: 2.87 Ga eclogites from the Kola Peninsula, Russia. Geology 38, 739-742.

Miyashiro, A., 1961. Evolution of metamorphic belts. J. Petrol. 2, 277–311.

Moyen, J.F., Stevens, G., Kisters, A., 2006. Record of mid-Archean subduction from metamorphism in Barberton Terrain, South Africa. Nature 442, 559–562

Newton, R.C., Charlu, T.V., ,Kleppa, O.J., 1980. Thermochemistry of the high structural state plagioclases. GeCA **44**, 933-41.

Park, R.G., 1982. Archaean tectonics. Geol. Rundsch. 71, 22–37.

Percival, J.A., Fountain, D.M., Salisbury, M.H., 1992. Exposed crustal cross sections as windows on the

lower crust. In: Fountain, D.M., Arculus, R.J., Kay, R.W. (Eds.), Continental Lower Crust. Elsevier, Amsterdam, 317–362.

Percival, J., 1994. Archean high-grade metamorphism. In: Condie, K.C. (Ed.), Archean crustal evolution. Developments in Precambrian Geology 1 1, Elsevier, 357-410..

Platt, J.P, and Visser, R.L.M., 1980. Extensional structures in anisotropic rocks. J. Struct. Geol. 2, 397-410.

Poujol, M., Robb, L.J., Respaut, J.P., Anhaeusser, C.R., 1996. 3.07–2.97 Ga greenstone belt formation in the northeastern Kaapvaal Craton: implications for the origin of the Witwatersrand Basin. Econ. Geol. 91 (8), 1455–1461.

Poujol, M., Respaut, J.P., Robb, L.J. and Anhaeusser, C.R., 1997. New U-Pb and Pb-Pb data on the Murchison greenstone belt, South Africa and their implications for the origin of the Witwatersrand basin. 319, EGRU, Johannesburg.

Poujol, M. and Robb, L.J., 1999. New U-Pb zircon ages on gneisses and pegmatite from South of the Murchison greenstone belt, South Africa. S. Afr. J. Geol., 102(2): 93- 97.

Poujol, M., 2001. U–Pb isotopic evidence for episodic granitoid emplacement in the Murchison greenstone belt, South Africa. J. Afr. Earth Sci. 33, 155–163.

Powell R., Holland T. J. B. and Worley B., 1998. Calculating phase diagrams involving solid solutions via non-linear equations, with examples using THERMOCALC. J. Metamorph. Geol. 16, 577-588.

Reno, B.L., Brown, M., Kobayashi, O.T., Nakamura, E., Piccoli, P.M. and Trouw, R.A.J., 2009. Eclogite–high-pressure granulite metamorphism records early collision in West Gondwana: New data from the Southern Brasília Belt, Brazil. J. Geol. Soc. Lond, 166, 1013-1032.

Rey, P.F., and Houseman, G., 2006. Lithospheric scale gravitational flow: the impact of body forces on orogenic processes from Archaean to Phanerozoic, In: Buiter, S. J. H. and Schreurs, G.(eds). Analogue and Numerical Modelling of Crustal Scale Processes. Geol. Soc. Lond. Spec. Publ., 253, 153–167.

Robb, L.J., Brandl, G., Anhaeusser, C.R., Poujol, M., 2006. Archaean Granitoid Intrusions, In: Johnson, M.R., Anhaeusser, C.R., Thomas, R.J., The Geology of South Africa, 2006.

Saha, L., Pant, N.C., Pati, J.K., Upadhyay, D., Berndt, J., Bhattacharya, A., Satynarayanan, M., 2011. Neoarchean high-pressure margarite–phengitic muscovite–chlorite corona mantled corundum in quartz-free high-Mg, Al phlogopite–chlorite schists from the Bundelkhand craton, north central India. Contrib. Mineral. Petrol. 161, 511–530.

Schwartz-Schampera, U., Terblanche, H., Oberthür, T., 2010. Volcanic-hosted massive sulfide deposits in the Murchison greenstone belt, South Africa. Mineralium Deposita 45, 2, 113-145.

Sizova, E., Gerya, T., Brown, M., Perchuk, L.L., 2010. Subduction styles in the Precambrian: insight from numerical experiments. Lithos 116, 3-4, 209-22.

Smith, D.C., 1984. Coesite in clinopyroxene in the Caledonides and its implications for geodynamics. Nature 310, 641–644.

South African Committee for Stratigraphy, 1980. Chapter 2.3: The Murchison Sequence, In*:* 559 C.L.E. Hart (Editor), Stratigraphy of South Africa, part 1: Lithostratigraphy of the 560 Republic of South Africa, South West Africa/Namibia and the Republics of 561 Bophuthatswana, Transkei and Venda. South Africa Geological Survey Handbook, 45-562 52.

Stacey, J.S and Kramers, J.D., 1975. Approximation of terrestrial lead isotope evolution by a two-stage model. Earth Planet. Sci. Lett. 26, 2, 207-221

Stüwe, K., 1997. Effective bulk composition change due to cooling: a model predicting complexities in retrograde reaction textures. Contrib. Mineral. Petrol. 129, 43–52.

Tajcmanová, L., Connolly, J.A.D., Cesare, B., 2009. A thermodynamic model for titanium and ferric iron solution in biotite. J. Metamorph. Geol. **27**, 153-64.

Van Kranendonk, M.J., Hickman, A.H., Smithies, R.H., Nelson, D.N., Pike, G., 2002. Geology and tectonic evolution of the Archaean North Pilbara terrain, Pilbara Craton, Western Australia. Econ. Geol. 97, 695–732.

Vearncombe, J.R., Barton, J.M. and Walsh, K.L. (1987). The Rooiwater Complex and associated rocks, Murchison granitoid-greenstone terrane, Kaapvaal Craton. S. Afr. J. Geol., 90, 361-377.

Vearncombe, J. R., Cheshire, P. E., De Beer, J. H., Killick, A. M., Mallinson, W. S., McCourt, S., et al., 1988a. Structures related to the Antimony line, Murchison schist belt, Kaapvaal craton, South Africa. Tectonophysics, 154 (3-4), 285-308.

Vearncombe, J. R., 1988b. Structure and metamorphism of the Archean Murchison Belt, Kaapvaal Craton, South Africa. Tectonics, 7(4), 761-774.

Vearncombe, J. R., Barton, J. M., Cheshire, P. E., De Beer, J. H., Stettler, E. H., and Brandl, G., 1992. Geology, geophysics and mineralization of the Murchison Schist Belt, Rooiwater Complex and surrounding granitoids, Memoir of the Geological Survey of South Africa, 81, 139p.

Viljoen, M.J, Van Vuuren, C.J.J., Pearton, P.N., Minnitt, R.C.A., Muff, R. and Cillier, P., 1978. The regional geological setting of mineralization in the Murchison Range with particular reference to antimony. In : Verwoerd, W.J. (Ed.), Mineralization in Metamorphic Terranes. Spec. Publ. Geol. Soc. S. Afr., 1, 661-668.

Volodichev, O., Slabunov, A., Bibikova, E., Konilov, A., Kuzenko, T., 2004. Archean eclogites in the Belomorian mobile belt, Baltic Shield. Petrology, 12, 540–560.

Waldbaum, D.R., Thompson, J.B., 1968. Mixing Properties Of Sanidine Crystalline Solutions .2. Calculations Based On Volume Data. Am. Min. **53**, 2000-?

Watts, A.B. and Burov, E.B., 2003. Lithospheric strength and its relationship to the elastic and seismogenic layer thickness. Earth Planet. Sci. Lett. 213, 113-131.

White, R.W., Powell, R., Holland, T.J.B., Worley, B.A. 2000b. The effect of TiO_2 and Fe_2O_3 on metapelitic assemblages at greenschist and amphibolite facies conditions: mineral equilibria calculations in the system K_2O-FeO-MgO-Al_2O_3-SiO_2-H_2O-TiO_2 Fe_2O_3. J. Metamorph. Geol. **18**:497-511.

Zeh, A., 2001. Inference of a detailed P-T path from P-T pseudosections using metapelitic rocks of variable composition from a single outcrop, Shackleton Range, Antarctica. J. Metamorph. Geol., 19, 329-350.

Zeh, A., Klemd, R., Buhlmann, S., Barton J.M., 2004. Pro- and retrograde P-T evolution of granulites of the Beit Bridge Complex (Limpopo Belt, South Africa): constraints from quantitative phase diagrams and geotectonic implications. J. Metamorph. Geol., 22, 79-95.

Zeh, A., 2006. Calculation of garnet fractionation in natural metamorphic rocks, with application to a flat-top, Y-rich garnet population from the Ruhla Crystalline Complex, Central Germany. J. Petrol., 47, 2335-2356.

Zeh, A., Gerdes, A. and Barton, J.M., 2009. Archean Accretion and Crustal Evolution of the Kalahari Craton - the Zircon Age and Hf Isotope Record of Granitic Rocks from Barberton/Swaziland to the Francistown Arc. J. Petrol., 50, 933-966.